

# 1 Impact of HO<sub>2</sub>/RO<sub>2</sub> ratio on highly oxygenated α-pinene 2 photooxidation products and secondary organic aerosol formation 3 potential

4 Yarê Baker<sup>1</sup>, Sungah Kang<sup>1</sup>, Hui Wang<sup>1</sup>, Rongrong Wu<sup>1</sup>, Jian Xu<sup>1</sup>, Annika Zanders<sup>1</sup>, Quanfu He<sup>1</sup>,  
5 Thorsten Hohaus<sup>1</sup>, Till Ziehm<sup>1</sup>, Veronica Geretti<sup>2</sup>, Thomas J. Bannan<sup>3</sup>, Simon P. O'Meara<sup>3,4</sup>, Aristeidis  
6 Voliotis<sup>3</sup>, Mattias Hallquist<sup>2</sup>, Gordon McFiggans<sup>3</sup>, Sören R. Zorn<sup>1</sup>, Andreas Wahner<sup>1</sup>, and Thomas F.  
7 Mentel<sup>1</sup>

8 <sup>1</sup>Institute for Energy and Climate Research, IEK-8, Forschungszentrum Jülich, 52425 Jülich, Germany

9 <sup>2</sup>Atmospheric Science, Dept. of Chemistry, University of Gothenburg, Gothenburg, 412 96, Sweden

10 <sup>3</sup>Department for Earth and Environmental Sciences, University of Manchester, Manchester, M13 9PL, UK

11 <sup>4</sup>National Centre for Atmospheric Science, University of Manchester, Manchester, M13 9PL, UK

12

13 *Correspondence to:* Thomas F. Mentel (t.mentel@fz-juelich.de)

14 **Abstract.** Highly oxygenated molecules (HOMHOMs) from the atmospheric oxidation of biogenic volatile organic  
15 compounds are important contributors to secondary organic aerosol (SOA). Organic peroxy radicals (RO<sub>2</sub>) and hydroperoxy  
16 radicals (HO<sub>2</sub>) are key species influencing the HOM product distribution. In laboratory studies experimental requirements  
17 often result in overemphasis of RO<sub>2</sub> cross-reactions compared to reactions of RO<sub>2</sub> with HO<sub>2</sub>. We analyzed the photochemical  
18 formation of HOMs from α-pinene and their potential to contribute to SOA formation under high (≈1/1) and low (≈1/100)  
19 HO<sub>2</sub>/RO<sub>2</sub> conditions. As HO<sub>2</sub>/RO<sub>2</sub> > 1 is prevalent in the daytime atmosphere, sufficiently high HO<sub>2</sub>/RO<sub>2</sub> is crucial to mimic  
20 atmospheric conditions and to prevent biases by low HO<sub>2</sub>/RO<sub>2</sub> on the HOM product distribution and thus SOA yield.  
21 Experiments were performed under steady-state conditions in the new, continuously stirred tank reactor SAPHIR-STAR at  
22 Forschungszentrum Jülich. The HO<sub>2</sub>/RO<sub>2</sub> ratio was increased by adding CO, while keeping the OH concentration constant.  
23 We determined the HOM's SOA formation potential, considering their fraction remaining in the gas phase after seeding with  
24 (NH<sub>4</sub>)<sub>2</sub>SO<sub>4</sub> aerosol. Increase of HO<sub>2</sub>/RO<sub>2</sub> led to a reduction in SOA formation potential, with the main driver being a ≈60%  
25 reduction in HOM-accretion products. We also observed a shift in HOM-monomer functionalization from carbonyl to  
26 hydroperoxide groups. We determined a reduction of the HOM's SOA formation potential by ≈30% at HO<sub>2</sub>/RO<sub>2</sub>≈1/1  
27 compared to HO<sub>2</sub>/RO<sub>2</sub>≈1/100. Particle phase observations measured an about according decrease in SOA mass and yield. Our  
28 study showed that too low HO<sub>2</sub>/RO<sub>2</sub> ratios compared to the atmosphere can lead to an overestimation of SOA yields.

## 29 1 Introduction

30 In the atmosphere highly oxidized products from the oxidation of biogenic or anthropogenic volatile organic compounds  
31 (VOCs) are an important source of secondary organic aerosol (SOA) (Roldin et al., 2019; Mohr et al., 2019). SOA is an  
32 important contributor to the overall ambient aerosol and of interest because of its impact on climate, visibility, and human  
33 health (Hallquist et al., 2009).

34 Recently, many studies (Pullinen et al., 2020; Berndt et al., 2016; Bianchi et al., 2017) have focused on understanding the  
35 oxidation pathways of VOCs that yield highly oxygenated molecules (HOMs), as these are expected to be of low enough  
36 volatility to condense into the particle phase. One important tool for the investigation of VOC degradation and SOA formation  
37 is the utilization of experiments in atmospheric simulation chambers (Hidy, 2019). Such experiments have also helped to  
38 elucidate key processes in the HOM formation, i.e. the process of autoxidation.

39 After an initial oxidant attack and the formation of a peroxy radical (RO<sub>2</sub>), autoxidation adds oxygen to the molecule via an  
40 internal H-shift to the peroxy group, forming a hydroxy peroxide group and an alkyl radical, to which O<sub>2</sub> immediately adds,  
41 reestablishing the peroxy functionality. This process can be repeated multiple times yielding almost instantaneously highly  
42 oxygenated peroxy radicals (HOM-RO<sub>2</sub>) which are terminated to a series of HOM closed-shell products (Bianchi et al., 2019;  
43 Ehn et al., 2014; Crouse et al., 2013).

44 Chamber studies often work with a singular compound and operate at higher precursor concentrations than those observed in  
45 the atmosphere for experimental reasons. These experiments cannot represent the complex mixture of VOCs and oxidized  
46 VOCs present in the atmosphere (McFiggans et al., 2019). Higher precursor concentrations can lead per se to higher SOA  
47 yields than observed in the atmosphere (a well characterized phenomenon (see Henry et al. (2012), Shilling et al. (2009)) and  
48 to a general preference of higher order processes which may not be important in the atmosphere. One example is that chamber  
49 studies tend to overestimate the role of cross reactions between organic peroxy radicals (RO<sub>2</sub>) owing to high precursor  
50 concentrations of a single VOC. In chambers, reactions of HOM-RO<sub>2</sub> with other organic peroxy radicals terminate the  
51 autoxidation chain, leading typically to multifunctional carbonyl and alcohol compounds. In comparison, in the atmosphere  
52 termination by HO<sub>2</sub> is more likely, leading to multifunctional hydroperoxides. In presence of sufficient NO, termination to  
53 multifunctional organic nitrates may be more important (Schervish and Donahue, 2021).

54 Another possible termination reaction of HOM-RO<sub>2</sub> with HOM-RO<sub>2</sub> and less oxidized RO<sub>2</sub> leads to the formation of accretion  
55 products, which are expected to be extremely low volatile organic compounds (ELVOCs) and are therefore expected to  
56 contribute to new particle formation and SOA formation (Ehn et al., 2014; Berndt et al., 2018). Schervish and Donahue (2021)  
57 raised awareness that chamber studies could overestimate the SOA formation potential from the oxidation of terpenes such as  
58  $\alpha$ -pinene compared to the atmosphere, because of missing HO<sub>2</sub> and small RO<sub>2</sub> (e.g. CH<sub>3</sub>O<sub>2</sub>), which favors accretion product  
59 formation. [Previous studies of VOC ozonolysis with different OH scavengers by Docherty and Ziemann \(2003\) and Keywood  
60 et al. \(2004\), indicated a significant impact of the HO<sub>2</sub>/RO<sub>2</sub> ratio on SOA yields.](#)

61 In chamber studies the use of higher VOC concentrations is often an unavoidable necessity either to match the sensitivity of  
62 the analytical instrumentation or to overcome chamber related effects. The question remains, how can conditions dictated by  
63 the chamber be steered towards more realistic chemical pathways and higher atmospheric relevance?

64 In this study we address this overestimated importance of peroxy radical cross reactions. We studied the photooxidation of  $\alpha$ -  
65 pinene in a series of steady-state experiments in the newly built continuously stirred tank reactor SAPHIR-STAR (a  
66 modernized version of JPAC, see Mentel et al. (2009)).

67 ~~In these experiments, after an initial  $\alpha$ -pinene photooxidation phase as a reference, CO was added to the oxidation system. We~~  
68 ~~compared two experimental conditions, a pure  $\alpha$ -pinene photooxidation case leading to low  $\text{HO}_2/\text{RO}_2$  ratios and high~~  
69 ~~importance of  $\text{RO}_2$  cross-reactions and a high  $\text{HO}_2/\text{RO}_2$  case representing more atmospheric relevant conditions with high~~  
70 ~~importance of  $\text{RO}_2 + \text{HO}_2$  reactions. One important concept of the conducted experiments is the constant OH availability to  $\alpha$ -~~  
71 ~~pinene in order to prevent effects of different oxidant levels and allow for a direct comparison between the two chemical~~  
72 ~~regimes. To this end, the OH concentration in the experiments was adjusted to keep the  $\alpha$ -pinene OH turnover constant and to~~  
73 ~~avoid changes due to oxidant scavenging.~~

74 ~~to represent small, oxidized VOCs in the atmosphere that can produce  $\text{HO}_2$  by reaction with OH (compare Schervish and~~  
75 ~~Donahue (2021)). Presence of CO shifts the  $\text{HO}_2$  to  $\text{RO}_2$  ratio, increasing the importance of the  $\text{RO}_2$  termination with  $\text{HO}_2$ .~~  
76 ~~However, McFiggans et al. (2019) showed that one limiting factor in mixture experiments is oxidant scavenging: the products~~  
77 ~~and their yields in mixed systems change, because there is less OH available to the individual VOC. Thus, after the CO addition~~  
78 ~~the OH production in the chamber was increased to compensate for the oxidant scavenging. The OH levels in the system before~~  
79 ~~and after the CO addition were approximately the same, keeping the  $\alpha$ -pinene OH turnover, as well as the primary peroxy~~  
80 ~~radical production approximately constant.~~

81 Furthermore, the addition of seed particles ( $(\text{NH}_4)_2\text{SO}_4$ ) allowed us to observe the condensation behavior of the HOM-products  
82 and to compare our gas phase observations directly with particulate phase measurements of the condensed organic mass.

83 In this study we will address two central questions: How does the shift in  $\text{HO}_2/\text{RO}_2$  impact the oxidation mechanism of  
84  $\alpha$ -pinene, especially the HOM formation pathway? And what is the subsequent impact on the SOA formation potential of the  
85  $\alpha$ -pinene photooxidation system? As the central analysis tool, we will use high resolution time of flight mass spectrometry  
86 with chemical ionization (HR-TOF-CIMS) ~~with nitrate ( $\text{NO}_3^-$ ) reagent ions as this ionization scheme is selective towards~~  
87 ~~HOM compounds (Hyttinen et al., 2018).~~

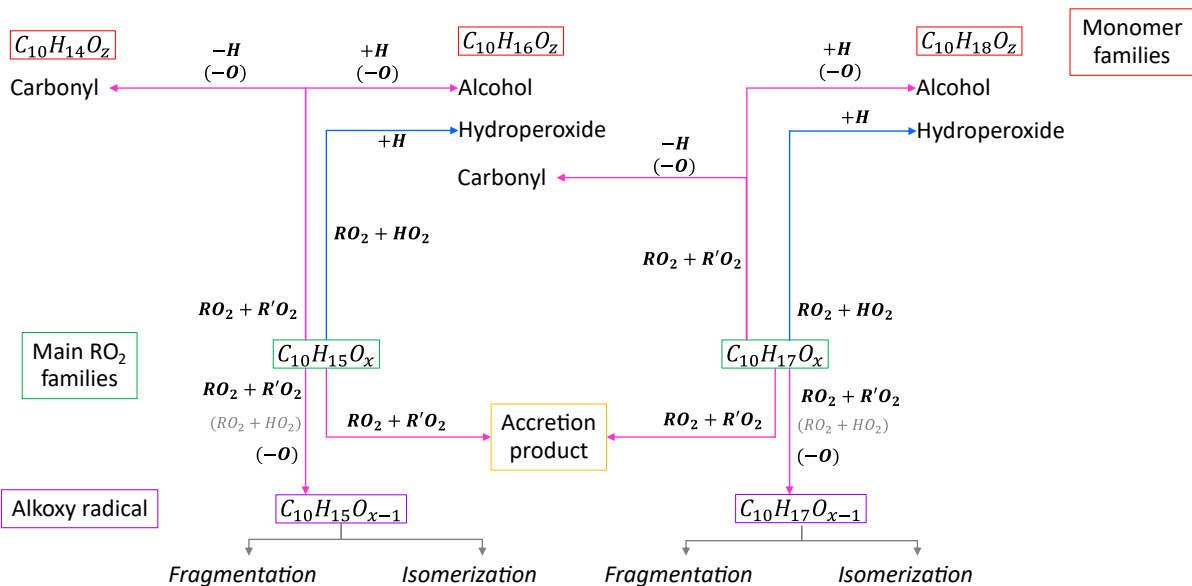
89 [1.12.1](#) Generic  $\alpha$ -pinene HOM peroxy radical chemistry

90 The chemical mechanistic information for the basic oxidation scheme of  $\alpha$ -pinene was taken from the Master Chemical  
91 Mechanism MCM v3.3.1 (Jenkin et al., 1997; Saunders et al., 2003) (<http://mcm.york.ac.uk>). The main peroxy radicals  
92 expected from  $\alpha$ -pinene photooxidation are  $C_{10}H_{17}O_x$  and  $C_{10}H_{15}O_x$ .  $C_{10}H_{17}O_x$  is formed by the addition of OH to  $\alpha$ -pinene,  
93 followed by  $O_2$  (starting  $RO_2$ :  $C_{10}H_{17}O_3$ ) (MCM v3.3.1 (Jenkin et al., 1997; Saunders et al., 2003)). Studies showed that the  
94 autoxidation can start from  $C_{10}H_{17}O_3$  with the four-member ring in  $\alpha$ -pinene opened (Berndt, 2021; Xu et al., 2019).

95 For  $C_{10}H_{15}O_x$  the autoxidation chain is assumed to start with  $C_{10}H_{15}O_4$ , which can be formed directly from ozonolysis via the  
96 vinyl hydroperoxide path (Johnson and Marston, 2008; Iyer et al., 2021) or via H-abstraction from first-generation oxidation  
97 products such as pinonaldehyde ( $C_{10}H_{16}O_2$ ). (MCM v3.3.1 (Jenkin et al., 1997; Saunders et al., 2003; Fantechi et al., 2002)). A  
98 recent study suggests direct H-abstraction by OH from  $\alpha$ -pinene (Shen et al., 2022): [as a starting point for the autoxidation](#)  
99 [chain](#).

100 The autoxidation process is rapid with H-shift rates of about  $0.01 - 0.1 \text{ s}^{-1}$  and faster (Piletic and Kleindienst, 2022; Berndt,  
101 2021; Xu et al., 2019; Vereecken et al., 2007). ~~Once the~~The autoxidation ~~process starts its~~chain will run quickly ~~adds, adding~~  
102 more oxygen to the molecule, until ~~the difficulty in abstracting remaining H atoms slows down the reaction sufficiently such~~  
103 ~~that~~bimolecular termination reactions ~~can~~are able to compete ~~with all available H-shift rates. The rate of an H-shift is~~  
104 [determined by the hydrogen's position in relation to the peroxy radical and the functional groups near the hydrogen and peroxy](#)  
105 [radical \(Otkjaer et al., 2018; Vereecken and Nozière, 2020\)](#). In the absence of  $NO_x$ , the peroxy radicals have two major  
106 bimolecular termination channels: the reaction with another  $RO_2$  or with  $HO_2$ . A third pathway is the intramolecular  
107 termination (Rissanen et al., 2014).

108 Based on the considerations above, we apply a simplified generic reaction scheme to analyze our observations. **Figure 1**  
109 shows an overview of the reaction pathways for the main peroxy radical families in the  $\alpha$ -pinene photooxidation and the  
110 resulting product groups and families. The compounds can be separated into four classes; peroxy radicals (HOM- $RO_2$ ),  
111 monomers (HOM-Mon), accretion products (HOM-Acc) and fragments (HOM-Frag). The HOM- $RO_2$  class consists of all  
112 detected HOM- $RO_2$ , with special focus on the analysis of the  $C_{10}$  HOM- $RO_2$  family. The HOM-Mon class contains the closed-  
113 shell HOM- $C_{10}$  products. The compounds in the fragment class contain less than ten carbon atoms, while all HOM-Acc  
114 compounds contain more than ten carbon atoms. The compound classes are further divided into groups and families. Here, the  
115 term group is used for compounds with the same carbon number, while a family contains all compounds with the same carbon  
116 and hydrogen number but a varying oxygen number.



117

118 **Figure 1: Overview of important reaction pathways of  $\alpha$ -pinene  $RO_2$  with other  $RO_2$  and  $HO_2$ .**

119 The termination of  $RO_2$  with  $HO_2$  will lead to hydroperoxide formation:



120 In the case of  $C_{10}H_{15}O_x$ , reaction (R1) will lead to multifunctional  $C_{10}H_{16}O_z$  hydroperoxides (wherein the notation  
 121 “hydroperoxides” or “carbonyls”, “alcohols” etc. here and in the following relates to the functionality of the group formed by  
 122 the termination reaction). For  $C_{10}H_{17}O_x$  it will lead to the formation of  $C_{10}H_{18}O_z$  hydroperoxides. The termination via  $RO_2 + RO_2$   
 123 can either result in the formation of accretion products or in the formation of carbonyls and alcohols. For the accretion product  
 124 formation, it is assumed that the two  $RO_2$  chemically bond eliminating  $O_2$  from the molecule:



125 Recombination reactions of the main peroxy radical families  $C_{10}H_{15}O_x$  and  $C_{10}H_{17}O_x$  lead to the product families  $C_{20}H_{30}O_z$   
 126 (combination of two  $C_{10}H_{15}O_x$ ),  $C_{20}H_{32}O_z$  (combination of  $C_{10}H_{15}O_x$  and  $C_{10}H_{17}O_x$ ), and  $C_{20}H_{34}O_z$  (combination of two  
 127  $C_{10}H_{17}O_x$ ).

128 However, due to reactions with smaller peroxy radicals, HOM-Acc families with smaller carbon and hydrogen numbers are  
 129 also observed. Indeed, one reason why the  $RO_2 + R'O_2$  termination is expected to affect the SOA formation potential is the  
 130 formation of accretion products by scavenging of less oxidized and smaller  $RO_2$  by HOM- $RO_2$ . Thus, the smaller  $RO_2$  will  
 131 also contribute to the SOA mass which would otherwise not be the case. For the HOM- $RO_2$  itself, it is expected that they  
 132 contribute to SOA formation independently of the termination pathway, due to the low volatility of its expected termination  
 133 products (Pullinen et al., 2020; McFiggans et al., 2019).

134 The second  $\text{RO}_2+\text{R}'\text{O}_2$  termination pathway is the formation of a carbonyl and alcohol compound:



135 In this reaction both radicals lose an oxygen atom, and a hydrogen atom is transferred to the  $\text{RO}_2$  forming the alcohol  
136 termination group. Preferences of  $\text{RO}_2$  to form an alcohol or carbonyl compound are possible for individual reactions, but  
137 statistically carbonyl and alcohols should be formed with the same fractions. Since mass spectrometry can only determine  
138 formula composition, we cannot distinguish alcohols and hydroperoxides, which arise from  $\text{RO}_2$  differing by one O atom.  
139 Therefore, details of balance of alcohol and carbonyl formation cannot be detected.

140 However, the formula composition can help to differentiate certain formation pathways. The  $\text{C}_{10}\text{H}_{14}\text{O}_z$  family contains only  
141 carbonyl formed from a  $\text{C}_{10}\text{H}_{15}\text{O}_x$   $\text{RO}_2$  while the alcohol will be part of the  $\text{C}_{10}\text{H}_{16}\text{O}_z$  family. The  $\text{C}_{10}\text{H}_{16}\text{O}_z$  family also contains  
142 the carbonyl produced from the  $\text{RO}_2+\text{R}'\text{O}_2$  monomer termination of  $\text{C}_{10}\text{H}_{17}\text{O}_x$ , while the alcohol from this  $\text{RO}_2$  family will be  
143 found in the  $\text{C}_{10}\text{H}_{18}\text{O}_z$  family. So, from a diagnostic point of view,  $\text{C}_{10}\text{H}_{14}\text{O}_z$  as well as  $\text{C}_{10}\text{H}_{18}\text{O}_z$  are uniquely related to a  
144 precursor radical family.

145 The classification of the formation pathways of the monomers is helpful to analyze the effect of the  $\text{HO}_2/\text{RO}_2$  ratio shift in the  
146 experiments. Considering the termination pathways, a decrease in the  $\text{C}_{10}\text{H}_{14}\text{O}_z$  family and an increase of the  $\text{C}_{10}\text{H}_{18}\text{O}_z$  family  
147 is expected with increasing  $\text{HO}_2/\text{RO}_2$  because of increasing termination by  $\text{HO}_2$  and decreasing termination by  $\text{RO}_2$ . In case of  
148  $\text{C}_{10}\text{H}_{18}\text{O}_z$  the increase of hydroperoxides is partially compensated by a decrease of the alcohol channel. For  $\text{C}_{10}\text{H}_{16}\text{O}_z$  the  
149 situation is more complicated as it contains contributions from all termination pathways.

150 Besides closed-shell products,  $\text{HOM-RO}_2$  can also form alkoxy radicals ( $\text{HOM-RO}$ ). In general, alkoxy radicals ( $\text{RO}$ ) are  
151 important intermediates in the oxidation scheme of organics and are formed via  $(\mathbf{R4})$  and probably also via  $(\mathbf{R5})$  for specific  
152  $\text{RO}_2$  (Jenkin et al., 2019):



153 In reaction  $(\mathbf{R5})$  OH will be formed. The importance of reaction  $(\mathbf{R5})$  compared to reaction  $(\mathbf{R1})$  is still unclear in the literature,  
154 but functionalization of the  $\text{RO}_2$  close to the peroxy functionality possibly enables this reaction (Iyer et al., 2018; Eddingsaas  
155 et al., 2012; Hasson et al., 2005; Jenkin et al., 2019). If reaction  $(\mathbf{R5})$  is of negligible importance, the reaction scheme will  
156 simplify and the effect of increased  $\text{HO}_2/\text{RO}_2$  is easier to diagnose.

157 We are interested in the importance of alkoxy radical formation as  $(\text{HOM})\text{-RO}$  tend to fragment, leading to the formation of  
158 smaller products (Vereecken et al., 2007). In the context of SOA formation, these fragments are less likely to contribute to  
159 SOA mass because of their higher volatility. Since alkoxy radicals are too unstable to be detected directly we use two diagnosis  
160 tools to judge the importance of  $\text{HOM-RO}$ . Firstly,  $\text{HOM-RO}$  fragmentation can lead to  $\text{HOM-RO}_2$  with less than 10 carbon

161 atoms which may also continue the autoxidation chain. Therefore, the abundance of HOM with less than 10 carbon atoms  
162 (HOM-Frag) indicates the importance of alkoxy steps. Secondly, with increasing functionalization, H-shifts retaining the  
163 carbon backbone become more likely (Vereecken et al., 2007) which will lead to a next generation of C<sub>10</sub>-HOM-RO<sub>2</sub>. Such  
164 alkoxy peroxy steps can continue the autoxidation chain (Mentel et al., 2015). Interestingly, by coupling of an alkoxy and a  
165 peroxy step, the parity of the number of oxygen atoms in the HOM-RO<sub>2</sub> changes, while in pure autoxidation steps the oxygen  
166 parity remains the same. Therefore, a parity change of the oxygen number can be used as an indication of alkoxy step  
167 abundance (Kang, 2021).

168 In summary we will use the changes in contribution and relative signal of the different families and classes to judge the impact  
169 of shifting from low to high HO<sub>2</sub>/RO<sub>2</sub> on the  $\alpha$ -pinene photooxidation pathway.

### 170 1.22.2 Control of $\alpha$ -pinene OH turnover

171 ~~After the initial  $\alpha$ -pinene photooxidation phase as a reference, CO was added to the oxidation system. The idea is to represent~~  
172 ~~small, oxidized VOCs in the atmosphere that can produce HO<sub>2</sub> by reaction with OH (compare Schervish and Donahue (2021)).~~  
173 ~~Presence of CO shifts the HO<sub>2</sub> to RO<sub>2</sub> ratio, increasing the importance of the~~ One important concept of the conducted  
174 ~~experiments is the constant OH availability to  $\alpha$  pinene in the mixtures with CO to avoid effects of oxidant scavenging~~  
175 ~~(McFiggans et al., 2019). Therefore, after each change in the HO<sub>2</sub>/RO<sub>2</sub> regime by CO addition, the OH level was readjusted~~  
176 ~~to yield the same  $\alpha$  pinene OH turnover and compensate for the OH consumed by CO. This OH adjustment ensures that the~~  
177 ~~primary  $\alpha$  pinene chemistry was kept the same and enables a direct comparison.~~

178 termination of RO<sub>2</sub> by HO<sub>2</sub>. McFiggans et al. (2019) showed that one limiting factor in mixture experiments is oxidant  
179 scavenging: the products and their yields in mixed systems change, because there is less OH available to the individual VOC.  
180 Thus, after the CO addition the OH production in the chamber was increased to compensate for the ~~OH consumed by CO. The~~  
181 ~~OH levels in the system before and after the CO addition were approximately the same, keeping the  $\alpha$ -pinene OH turnover~~  
182 ~~approximately constant. This OH adjustment ensures that the primary  $\alpha$ -pinene chemistry was kept the same, avoiding effects~~  
183 ~~by different oxidant levels, and enabling a direct comparison.~~

184 However, since experiments could only be performed at *about* the same OH levels, a normalization by the actual  $\alpha$ -pinene OH  
185 turnover is applied to the data. This compensates for the slight experimental imperfections and enables better comparison of  
186 experiment series with different boundary conditions. The turnover in steady state is given in **Eq. (1)**. Here the subscript “SS”  
187 denotes steady state condition for the concentrations of  $\alpha$ -pinene and OH,  $k_{OH}$  is the  $\alpha$ -pinene OH reaction rate constant.

$$turnover_{\alpha\text{-pinene}+OH} = k_{OH} * [\alpha\text{-pinene}]_{SS} * [OH]_{SS} \quad (1)$$

188 This normalization also directly shows the yield of certain oxidation product or product group per  $\alpha$ -pinene consumed by OH.

189 **1.3.2.3 Derivation of effect on condensable mass from gas-phase measurement**

190 A simple proxy for the condensable mass from HOM products can be calculated from the steady-state HOM-signals measured  
191 by the NO<sub>3</sub>-CIMS, assuming condensation for all low volatility HOM-compounds and no back evaporation into the gas phase.  
192 To only take low volatility products into account we used all detected formula compositions with M > 230 g mol<sup>-1</sup> and weighted  
193 them with their molar mass. The reasoning behind this threshold can be found in **Sect. 4.4**. All contributions were summed up  
194 and normalized with the α-pinene OH turnover for the comparison between the low and high HO<sub>2</sub>/RO<sub>2</sub> cases (**Eq. (2)**).

$$mass\ weighted\ signal\ sum = \frac{\sum_{i=0}^i S_i * M_i}{turnover_{\alpha\text{-pinene}+OH}} \quad (2)$$

195 We also estimated the expected SOA mass formed using the calibration factor obtained for sulfuric acid for our NO<sub>3</sub>-CIMS  
196 instrument in a calibration setup (see supplement **Sect. S1**). From this we calculated an upper boundary concentration of  
197 detected HOM-compounds in the gas phase under the assumption that sulfuric acid clusters with nitrate at the collision limit,  
198 yielding maximum sensitivity (a common approach, see for example Ehn et al. (2014), Pullinen et al. (2020)).

199 The calculated gas phase concentration was then used in the steady state equation describing the relationship between gas and  
200 particle phase concentrations of a single compound *i* shown in **Eq. (3)**.

$$m_{i,seed}(p) = \frac{m_{i,seed}(g) * k_{cond,i}}{k_{particleLoss} + k_{evap,i}} \quad (3)$$

201 **Equation (3)** shows that the steady state particle phase (mass) concentration  $m_{i,seed}(p)$  of compound *i* in presence of seed in  
202 the chamber is only dependent on the steady state gas phase concentration  $m_{i,seed}(g)$ , the condensation rate and evaporation  
203 rate constants  $k_{cond,i}$ ,  $k_{evap,i}$  of *i* (to and from the particles) and the particle loss rate constant  $k_{particleLoss}$  in the chamber.

204 The condensation rate can be calculated (see supplement **Sect. S6S8**), and the particle loss rate constant was measured by  
205 observation of the particle loss in the chamber after ending the seed addition (details in the supplement **Sect. S2**). The  
206 evaporation rate was assumed to be negligible for the investigated HOM-compounds.

207 For the SOA yield calculation, we calculate a corrected organic mass  $m_{SOA}$  from the organic mass  $m_{AMS}$  measured by aerosol  
208 mass spectrometry (AMS) and the fraction expected to be lost on the seed particles compared to the overall loss on particles  
209 and chamber wall as shown in **Eq. (4)** (McFiggans et al., 2019).

$$m_{SOA} = m_{AMS} * \frac{k_{cond} + k_{wall}}{k_{cond}} \quad (4)$$

210 In **Eq. (4)** we use the condensation rate constant  $k_{cond}$  calculated for one major HOM-product (C<sub>10</sub>H<sub>16</sub>O<sub>7</sub>) and the average  
211 HOM-Mon wall loss rate  $k_{wall}$  which was determined by switching off the UVC light and observing the decay of  
212 photooxidation products in the NO<sub>3</sub>-CIMS. The wall loss determination, as well as SOA mass correction were described before  
213 in Sarrafzadeh et al. (2016) and McFiggans et al. (2019).



## 214 **23** Experimental methods

### 215 **2.13.1** Chamber setup

216 Experiments were conducted in the Jülich SAPHIR STAR chamber, which is the modern successor of the JPAC setup (Mentel  
217 et al., 2009). The basic concepts are the same as in JPAC, but each parameter is set, controlled, and monitored in a program.  
218 The chamber was operated as a continuously stirred tank reactor. It is a borosilicate glass cylinder ( $l=2.5$  m,  $d=1$  m) with a  
219 volume of close to 2000 L and all equipment inside the chamber is either glass or glass coated steel (SilcoTek GmbH).

220 With an inflow of  $32 \text{ L min}^{-1}$ , the residence time in the chamber was approximately ~~6361~~ minutes with a fan ensuring mixing  
221 within minutes. In contrast to the JPAC chamber, the stirring is conducted perpendicular to the cylinder axis, as opposed to  
222 coaxial. Chamber inflow is split into two humidified clean air flows (mixed from  $\text{N}_2$  and  $\text{O}_2$ ) of about equal volume, one with  
223 added oxidant (here  $\text{O}_3$ ), the other with added VOC and other trace gases (here  $\alpha$ -pinene and CO). All experiments were  
224 performed at a relative humidity of 50 % and at  $20^\circ\text{C}$ . Temperature stability is ensured by the climate-controlled surrounding  
225 of the chamber.

226  $\alpha$ -Pinene ( $\geq 99$  % purity, Sigma-Aldrich Merck KGaA) was introduced via liquid injection with a syringe pump (Fusion 4000,  
227 CHEMYX Inc.) into a heated glass bulb and flushed by a stream of  $1 \text{ L min}^{-1}$  into the chamber. CO was added from a gas  
228 bottle (10% CO in  $\text{N}_2$ , Messer SE & Co. KGaA). Ozone was directly produced photolytically before injection with a self-built  
229 ozone generator.

230 OH is produced in the chamber by ozone photolysis using two UV-C lamps with a wavelength of 254 nm and subsequent  
231 reaction of  $\text{O}(^1\text{D})$  with water vapor. The lamps are mounted in closed quartz cylinders in the middle of the chamber, vertically  
232 to the cylinder axis and light intensity can be varied with a movable shielding installed around the lamps. The shielding allows  
233 an exact percentage of the lamp to be covered, thus controlling the amount of OH produced in the chamber.

234 The OH radical concentration after CO addition was adjusted by setting the shielding of the UVC lamps and a slight adjustment  
235 of  $\text{O}_3$  inflow. The applied  $J(\text{O}^1\text{D})$  values in different phases were calculated to be in the range of  $0.8 \cdot 10^{-3}$  to  
236  $2.4 \cdot 10^{-3} \text{ s}^{-1}$ .

237 In some of the experiments, ammonium sulfate ( $\geq 99$  % purity, Merck KGaA) seed particles were added to the system to  
238 provide a surface for the condensation of organic material. The aerosol was produced with a modified TSI atomizer (Model  
239 3076, TSI GmbH) and dried to 50% relative humidity.

240 VOC concentrations in the chamber were measured using proton-transfer-reaction mass spectrometry (PTR-TOF-MS; Ionicon  
241 GmbH).  $\text{CO}_2$ , CO,  $\text{H}_2\text{O}$  (G2401 Cavity Ringdown Spectrometer, Picarro Inc.), NO,  $\text{NO}_x$  (NCLD899, Eco Physics GmbH with  
242 a home-built photolytic converter) and  $\text{O}_3$  (O342e, Envea GmbH) were additionally monitored. Particle distribution and  
243 concentration were measured with a condensation particle counter (CPC, Model 3788, TSI GmbH) and a scanning mobility

244 particle sizer (SMPS; Model 3080, TSI GmbH) with a CPC (Model 3788, TSI GmbH). The aerosol composition was measured  
245 with a high-resolution aerosol mass spectrometer (HR-TOF AMS; Aerodyne Inc.).

246 In all experiments, VOC, O<sub>3</sub>, and SMPS+CPC sampling switched between inlet and outlet of the chamber to measure the input  
247 concentrations as well as the concentrations in the reactor. The flow control system of the chamber adapts to these switches so  
248 that the inflow into the chamber stays constant.

249 All results discussed here were observed under steady-state conditions when all parameters were constant. For each steady  
250 state, the OH concentration was calculated from the decay of  $\alpha$ -pinene as described by Kiendler-Scharr et al. (2009). **Equation**  
251 **(5)** is derived from the mass balance of  $\alpha$ -pinene at steady state. The steady state OH concentration [OH]<sub>SS</sub> depends on the  
252 amount of  $\alpha$ -pinene consumed by reaction with OH and the reaction with O<sub>3</sub>, as well as the flush out.

$$[OH]_{SS} = \frac{F}{V} * \frac{[VOC]_{in} - [VOC]_{SS} - k_{O_3} * [O_3]_{SS}}{k_{OH}} \quad (5)$$

253 Here, F is the total flow and V the volume of the chamber. The subscript “SS” indicates steady-state concentrations, while  
254 [VOC]<sub>in</sub> represents the  $\alpha$ -pinene concentration entering the chamber. k<sub>o3</sub> and k<sub>OH</sub> represent the reaction rate constants of  $\alpha$ -  
255 pinene with the corresponding oxidant. We applied rate coefficients of  $k_{o_3}k_{OH}=5.36 \cdot 10^{-11} \text{ cm}^3 \cdot \text{s}^{-1}$  (Atkinson and Arey, 2003)  
256 and  $k_{OH}k_{O_3}=9.25 \cdot 10^{-17} \text{ cm}^3 \cdot \text{s}^{-1}$  (Cox et al., 2020) at 20 °C. The uncertainty of the OH calculation was estimated as 20 % by  
257 Wildt et al. (2014).

258

259 **2.23.2 Experiment conditions**

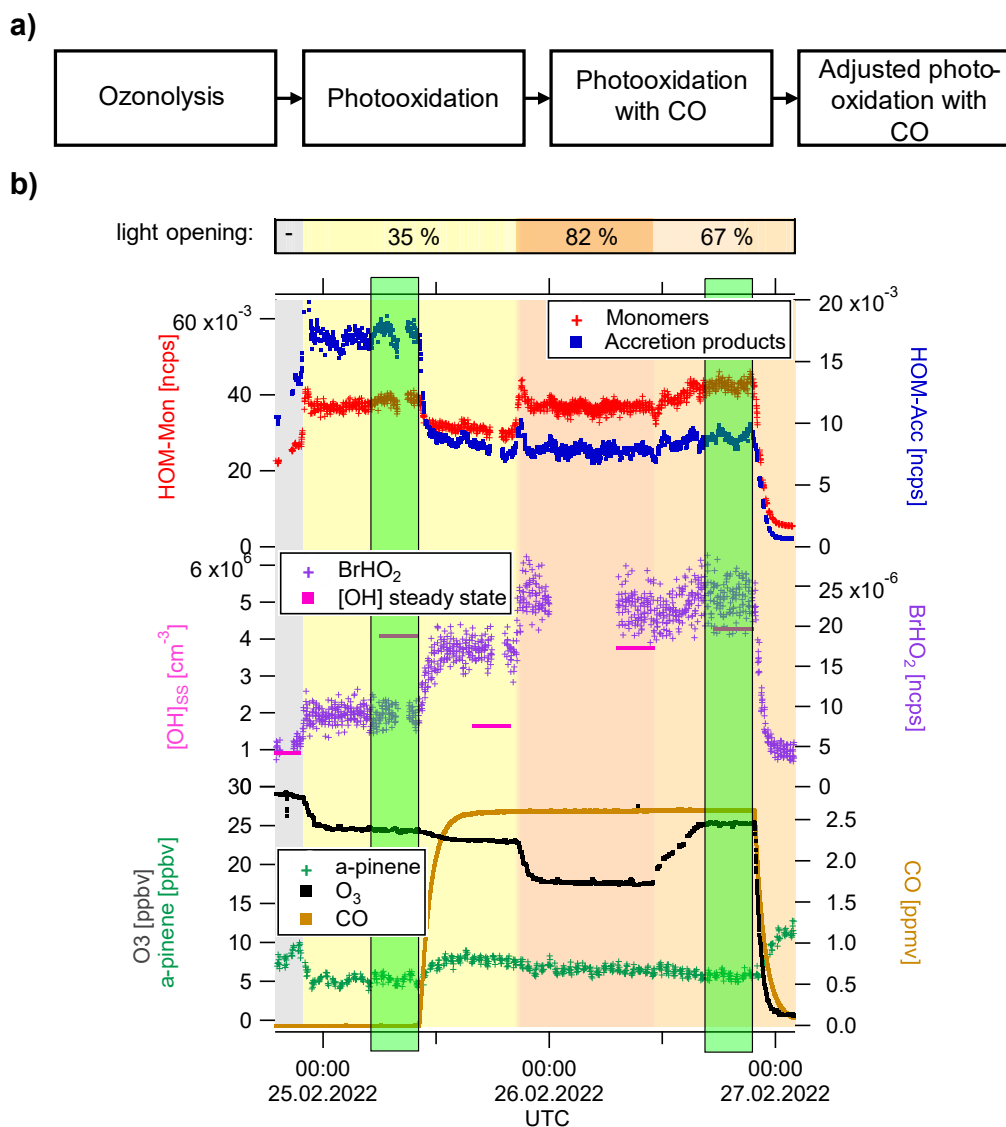
260 An overview of the experiments and their boundary conditions can be found in **Table 1**. Four experiments were performed in  
 261 total, leading to one repetition of each studied condition. In two of the experiments ammonium sulfate seeds were added  
 262 leading to a total particle surface in the chamber on the order of  $8 \cdot 10^{-4} \text{ m}^2 \text{ m}^{-3}$  and organic loadings of about  $3 \text{ ug m}^{-3}$  in the  
 263 photooxidation stage. In the unseeded experiments no significant nucleation was observed leading to pure gas phase conditions.  
 264 The *Exp2* experiment is a consecutive combination of a seeded, followed by a non-seeded experiment to provide direct insight  
 265 into the effect of seed presence on the system.

266 As the OH radical is produced by photolysis of ozone and  $\alpha$ -pinene reacts with ozone, it is important to know the relative  
 267 contribution of the  $\alpha$ -pinene consumption by OH and by  $\text{O}_3$ . This is achieved by comparing the turnover of  $\alpha$ -pinene with OH  
 268 and  $\text{O}_3$  respectively. The results can be found in **Table 1**. The listed results are for the low  $\text{HO}_2/\text{RO}_2$  conditions, but nearly  
 269 identical values were reached after the  $\text{HO}_2/\text{RO}_2$  shift.

270 **Table 1. Overview of experimental conditions**

Name	Experiment description	[VOC] <sub>in</sub>	[CO] <sub>in</sub>	[OH] <sub>ss</sub> at low $\text{HO}_2/\text{RO}_2$	Contribution of OH to turnover at low $\text{HO}_2/\text{RO}_2$	Particle surface at low $\text{HO}_2/\text{RO}_2$	Organic mass concentration at low $\text{HO}_2/\text{RO}_2$
<i>Exp1</i>	<i>pure gas phase unseeded (1)</i>	10 ppbv	2.5 ppmv	$4.1\text{E}+6 \text{ cm}^{-3}$	80 %	-	-
<i>Exp2.1</i>	<i>seeded (1)</i>	10 ppbv	2.5 ppmv	$1.0\text{E}+7 \text{ cm}^{-3}$	91 %	$8.7\text{E}-4 \text{ m}^2 \text{ m}^{-3}$	$3.4 \text{ ug m}^{-3}$
<i>Exp2.2</i>	<i>unseeded (2)</i>	10 ppbv	2.5 ppmv	$1.3\text{E}+7 \text{ cm}^{-3}$	93 %	-	-
<i>Exp3</i>	<i>seeded (2)</i>	10 ppbv	2.5 ppmv	$1.4\text{E}+7 \text{ cm}^{-3}$	79 %	$6.8\text{E}-4 \text{ m}^2 \text{ m}^{-3}$	$2.7 \text{ ug m}^{-3}$

271



273

274 **Figure 2:** a) Experiment flow scheme b) Exemplary timeseries of *ExpI* experiment showing HOM-Mon and HOM-Acc  
 275 product sum (top panel), calculated OH concentration and BrHO<sub>2</sub> signal (middle panel), and ozone,  $\alpha$ -pinene and CO  
 276 concentrations (bottom panel). Background color represents light intensity. Highlighted in green are the low HO<sub>2</sub>/RO<sub>2</sub> steady  
 277 state and the steady state at high HO<sub>2</sub>/RO<sub>2</sub> (addition of CO and adjusted oxidant level).

278 All experiments started with  $\alpha$ -pinene ozonolysis followed by illumination of the UVC-lights to induce the reaction with OH.

279 A general flow scheme of the experiment can be found in **Fig. 2**, together with one exemplary timeseries of the unseeded

280 experiment *ExpI*. After the photooxidation steady state, CO was added to the system. In the displayed *ExpI* experiment the

281 OH concentration-level was adjusted in three steps to approach the desired-valuesame concentration as before the CO addition.

282 First the UVC-light opening was adjusted and then O<sub>3</sub> was added, and the UVC-light opening was adjusted again. In some

283 experiments initially the effect of CO on the unchanged system was observed, before the adjustment of OH. In other  
284 experiments (*Exp2.2*, *Exp3*) the adjustment of the  $\alpha$ -pinene OH turnover via ozone concentration and UVC-light opening were  
285 made simultaneously with the CO addition. Highlighted in green are the steady states with the “same” OH concentration  
286 characterized by low and high HO<sub>2</sub>/RO<sub>2</sub>, which were used for analysis and interpretation.

#### 287 [2-43.4](#) Model calculation for HO<sub>2</sub>/RO<sub>2</sub> ratio estimation

288 Box model calculations were performed applying the MCM v3.3.1 chemistry (Jenkin et al., 1997; Saunders et al., 2003) under  
289 the boundary conditions of the SAPHIR-STAR chamber. All calculations were performed with the institute software package  
290 EASY which uses FACSIMILE to solve the differential equations (EASY Version 5.69b). More details about the model  
291 parameters can be found in the supplement **Sect. S3**. The model calculations reproduced the primary observables  $\alpha$ -pinene,  
292 O<sub>3</sub>, CO, and OH within the experimental uncertainties. The box-model results were used to characterize the HO<sub>2</sub>/RO<sub>2</sub> ratio of  
293 the chemical systems, as no direct measurement of these parameters was available. The observed cluster signal BrHO<sub>2</sub><sup>-</sup> follows  
294 the modelled HO<sub>2</sub> concentration (**Fig. 3**).

295 The model predicts a shift of the HO<sub>2</sub>/RO<sub>2</sub> ratio from about 0.01 to about 1 by CO addition and oxidant adjustment, an increase  
296 by two orders of magnitude. Owing to lack of observations to verify model results, we will consider only the magnitude of  
297 HO<sub>2</sub>/RO<sub>2</sub> here. The model results show that indeed a major shift from RO<sub>2</sub>+RO<sub>2</sub> to RO<sub>2</sub>+HO<sub>2</sub> reactions can be expected.

298 We further used the modelled RO<sub>2</sub> and HO<sub>2</sub> concentrations to estimate the relative importance of pathways for individual  
299 (observed) HOM-RO<sub>2</sub>. For that we applied two generic rate coefficients  $k_{RO_2HO_2}$  and  $k_{RO_2RO_2}$ . As the rate coefficient for the  
300 RO<sub>2</sub>+HO<sub>2</sub> termination to a hydroperoxide  $k_{RO_2HO_2}$  we used the value specified in the MCM (~~1.852.46~~  $10^{-11}$  cm<sup>3</sup>·s<sup>-1</sup> at 20 °C  
301 (Jenkin et al., 1997; Saunders et al., 2003)). We chose a  $k_{RO_2RO_2}$  of  $5 \cdot 10^{-12}$  cm<sup>3</sup>·s<sup>-1</sup> as the approximated reaction rate of the  
302 RO<sub>2</sub>+RO<sub>2</sub> reactions. This value applies to all possible reactions (accretion product, monomer, and alkoxy formation) and is in  
303 the range of  $k_{RO_2RO_2}$  utilized by Roldin et al. (2019) in the PRAM model.

#### 304 [2-53.5](#) Determination of oxidized VOCs, HOMs and HO<sub>2</sub>

305 Chemical ionization mass spectrometry (HR-TOF-CIMS) techniques were used to detect a range of gaseous compounds. For  
306 this, two atmospheric pressure interface time of flight mass spectrometers (APi-TOF-MS; ToFwerk AG) with different inlet  
307 systems were used simultaneously. General information about the APi-TOF-MS instrument can be found in Junninen et al.  
308 (2010).

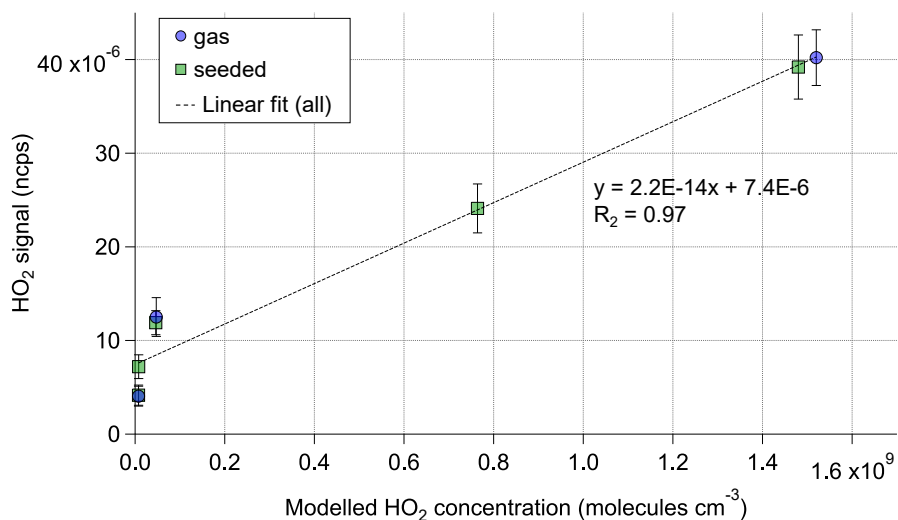
309 A long TOF (LTOF) (Resolution ~8500 for peaks at >200 m/Q) was coupled with the multi-scheme ionization inlet (MION;  
310 Karsa Oy). The setup of the inlet is described in detail by Rissanen et al. (2019). The distinctive feature of the MION inlet is  
311 the switching between two reagent ions. Here, nitrate was used to detect closed-shell HOMs, as well as HOM-RO<sub>2</sub>. Bianchi et  
312 al. (2019) suggested to define HOM as products stemming from autoxidation containing more than 6 oxygen. In our overall  
313 analysis we decided to also include fragments and monomers containing 5 or in a few cases 4 oxygens (see peaklist in

314 supplement **Sect. S4S5**) as we are interested to see if the importance of these less oxidized (but still with NO<sub>3</sub>-CIMS detectable)  
315 products increases at higher HO<sub>2</sub>/RO<sub>2</sub>. However, in all considerations regarding SOA formation we furthermore set a molar  
316 weight threshold which automatically excluded any products with less 6 oxygens.

317 As the second reagent ion, bromide was used to detect less oxidized products and the HO<sub>2</sub> radical (Albrecht et al., 2019;  
318 Sanchez et al., 2016). The nitrate ion source had a reaction time of 600 ms, while the bromide ion source had a shorter reaction  
319 time of 60 ms. For all experiments an inlet flow of 10 L min<sup>-1</sup> was used and the ionization scheme was switched every  
320 10 minutes.

321 In the data evaluation the first step was the separation of the timeseries of the two reagent ions. The data was subsequently  
322 processed with Tofware (Version 3.2.3, ToFwerk AG) using the high resolution timeseries workflow. No transmission  
323 correction was performed as previous measurements showed an approximately flat relative transmission curve in the mass  
324 region of interest. The analyte signals were normalized with the reagent ion signal (NO<sub>3</sub><sup>-</sup> and HNO<sub>3</sub>NO<sub>3</sub><sup>-</sup> for nitrate and Br  
325 and BrH<sub>2</sub>O for bromide).

326 Since no direct HO<sub>2</sub> calibration was available, the HO<sub>2</sub> signal in the Br-MION-CIMS was used to compare the levels of HO<sub>2</sub>  
327 relative to each other in the different phases of the experiment. The comparison of the measured HO<sub>2</sub> signal to the modelled  
328 HO<sub>2</sub> concentration shows a good linear relation between the model predictions and observations.



329

330 **Figure 3: Modelled HO<sub>2</sub> concentration vs. normalized HO<sub>2</sub> signal for each steady state of Exp2. HO<sub>2</sub> is measured as the BrHO<sub>2</sub>**  
331 **cluster and is normalized with the sum of the reagent ion Br<sup>-</sup> and its water cluster. The dotted line shows the linear fit to all (gas**  
332 **phase and seeded) measurement points.**

333 **Figure 3** illustrates this for the example of the Exp2 experiment. A background signal of around ~1·10<sup>-5</sup> is observed as soon  
334 as VOC and ozone are present in the reactor. The background HO<sub>2</sub> signal was not observed when only O<sub>3</sub> or only VOC were

335 in the system. As shown by the MCM modelling results HO<sub>2</sub> production of this strength is not expected in the α-pinene  
336 ozonolysis phase but this background phenomenon was observed before (Albrecht et al., 2019) and is not fully understood.

337 For the HOM molecules measured by the NO<sub>3</sub>-MION-CIMS the relative changes between different experiment phases are  
338 compared. For all detected HOM products the same detection sensitivity is assumed. ~~Hyttinen et al. (2018)~~[Hyttinen et al.](#)  
339 [\(2018\)](#) showed in quantum chemical calculations that HOMs containing 6 or more oxygen atoms have comparable sensitivity  
340 with the nitrate reagent ion. At this degree of oxidation it can be expected that the HOMs already contain multiple hydroperoxyl  
341 and/or hydroxy functional groups (Bianchi et al., 2019) prior to the termination step, making it unlikely that the sensitivity is  
342 strongly influenced by the termination group. Thus, the signal strength reflects the correct ranking of the observations and  
343 relative comparisons do not require calibration. Pullinen et al. (2020) studied the mass balance between condensable HOMs  
344 and formed particle mass and were able to find closure within a factor of 2.

345 A second CI-APi-TOF was used to measure less oxidized species. It was configured with a CI inlet based on the design of  
346 Eisele and Tanner (1993) coupled to an HTOF (Resolution ~2700 for peaks at >200 m/Q) (Tofwerk AG) and was operated in  
347 positive mode with propylamine (C<sub>3</sub>H<sub>7</sub>NH<sub>2</sub>, Sigma-Aldrich, purity ≥99%) to detect the early generation RO<sub>2</sub> and oxidation  
348 products (Berndt et al., 2018). The propylamine was purified and added as an amine-N<sub>2</sub> mixture (flow: 0.12 mL min<sup>-1</sup>) to the  
349 30 L min<sup>-1</sup> sheath flow. Furthermore, the sheath flow air is humidified to optimize ionization. The instrument sampled  
350 0.1 L min<sup>-1</sup> from the chamber, which was diluted with 9.9 L min<sup>-1</sup> for a sample flow of 10 L min<sup>-1</sup>. The dilution was necessary  
351 to reduce depletion of the primary ion (Hantschke, 2022).

## 352 [34](#) **Results and Discussion**

353 In order to understand the effect of HO<sub>2</sub>/RO<sub>2</sub> on the gas phase product composition, we will present and compare two cases:  
354 The steady state without CO (low HO<sub>2</sub>/RO<sub>2</sub>) and the steady state with CO addition and OH adjustment by J(O<sup>1</sup>D) and O<sub>3</sub> (high  
355 HO<sub>2</sub>/RO<sub>2</sub>). The modelling results predicted HO<sub>2</sub>/RO<sub>2</sub> of about 1/100 and of about 1/1 for these two cases respectively. [The](#)  
356 [modelled concentrations can be found in supplement Sect. S4](#). The modelling results show that the HO<sub>2</sub>/RO<sub>2</sub> ratio changes by  
357 two orders of magnitude, because [RO<sub>2</sub>] was reduced by about a factor of three, while [HO<sub>2</sub>] was increased by a factor of 30.  
358 Consequently, HO<sub>2</sub> reactions were almost negligible at low HO<sub>2</sub>/RO<sub>2</sub> while RO<sub>2</sub>+RO<sub>2</sub> reactions can still contribute at high  
359 HO<sub>2</sub>/RO<sub>2</sub>.

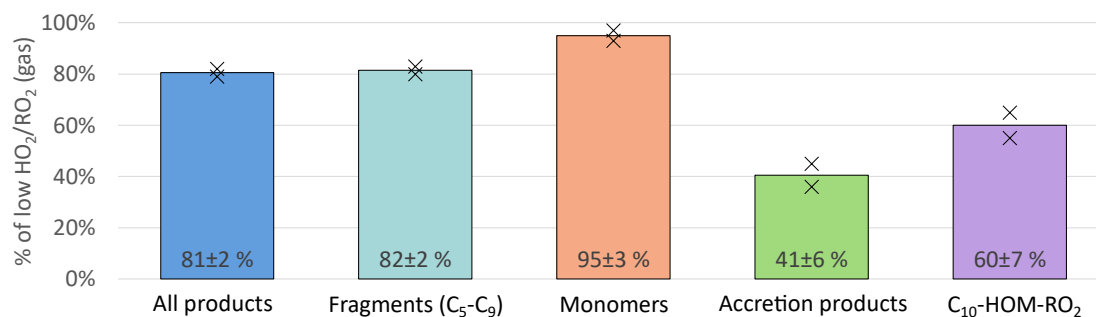
360 [HO<sub>2</sub>/RO<sub>2</sub> ratios of around 1 are highly relevant for atmospheric conditions with significant OH oxidation, though it should be](#)  
361 [kept in mind that in atmospheric conditions the methyl peroxy radical and other small RO<sub>2</sub> contribute a significant portion to](#)  
362 [the total of peroxy radicals \(Khan et al., 2015\). Field studies reporting HO<sub>2</sub> and RO<sub>2</sub> measurements for different environments](#)  
363 [can be found in supplement Table S5. These exemplary studies show that HO<sub>2</sub>/RO<sub>2</sub> ratios around 1 are relevant in remote to](#)  
364 [urban environments with different VOC sources and NO<sub>x</sub> levels.](#)

365 Assuming correctly modelled  $[HO_2]$  and  $[RO_2]$ , we calculated the competition between  $HO_2$  and  $RO_2$  reactions for each  
 366 (observed)  $RO_2$  expressed in form of pseudo first order rate coefficients in  $k_{RO_2HO_2} \cdot [HO_2]$  or  $k_{RO_2RO_2} \cdot [RO_2]$ . Herein  $[RO_2]$   
 367 is the sum of all  $RO_2$  species as defined in the MCM v3.3.1. For all experiments the results of our calculations indicate that  
 368 the sink for HOM- $RO_2$  is dominated by  $RO_2+RO_2$  reactions at low  $HO_2/RO_2$  (~9897 % contribution), while at high  $HO_2/RO_2$   
 369  $RO_2+HO_2$  contributed ~75 %. As the rate coefficients are not well known and we cannot verify the modelling results for  $HO_2$   
 370 and  $RO_2$  our calculations serve solely as an indication of expected trends in the chemical system.

### 371 3.14.1 Impact on overall HOM-formation

372 The top panel of **Fig. 2** shows the timeseries of HOM-Mon and HOM-Acc products. The HOM-Mon signal recovers after  
 373 the oxidant adjustment, while the HOM-Acc signal is significantly suppressed at high  $HO_2/RO_2$ . This indicates that the shift  
 374 from low to high  $HO_2/RO_2$  substantially impacts the termination reactions, shifting formation from the HOM-Acc product  
 375 channel ( $RO_2+RO_2$ ) to the HOM-Mon channel.

376 An overview of the results for the product classes defined in the method section is shown in **Fig. 4**. Plotted are the average  
 377 ratios of signal in the  $NO_3$ -CIMS in the high  $HO_2/RO_2$  steady state compared to the low  $HO_2/RO_2$  steady state. For better  
 378 comparison, all experiment phases were normalized to the actual  $\alpha$ -pinene OH turnover. The overall HOM-signal was lower  
 379 at high  $HO_2/RO_2$  showing a reduction of about 20 %. Most distinctive, the HOM-Acc were strongly reduced by about 60 %.  
 380 A reduction of HOM-Acc by addition of CO was observed before by McFiggans et al. (2019), however there the OH  
 381 concentration was not kept constant. The HOM-Frag ( $5 \leq C < 10$ ) also show a reduction of about 20 %. At high  $HO_2/RO_2$   
 382  $C_{10}$ -HOM- $RO_2$  were also reduced significantly by about 40 %.



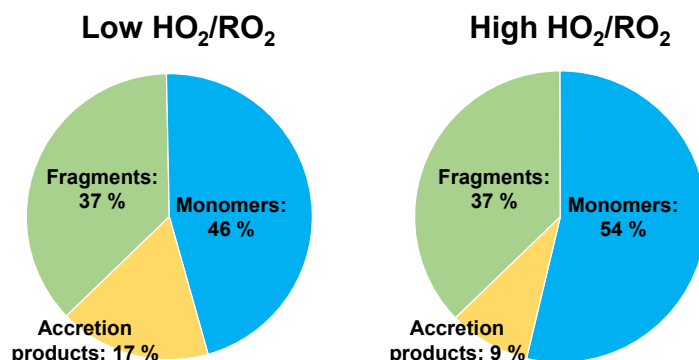
383

384 **Figure 4: Overview of average, relative change in product classes detected in  $NO_3$ -CIMS between low and high  $HO_2/RO_2$  case (both**  
 385 **normalized to  $\alpha$ -pinene OH turnover) for pure gas phase unseeded experiments. Bars represent average of the two experiments,**  
 386 **markers represent individual experiments.**

387 The HOM-Mon signal level remained about the same at low and high  $HO_2/RO_2$ . Without changes in the rates and contributions  
 388 of the different termination reactions, the observed reduction in the HOM- $RO_2$  precursors should lead to nearly the same  
 389 reduction of HOM-Acc in HOM-Mon. However, the decrease of accretion product formation and fragmentation should lead to  
 390 an increase in HOM-Mon, as each HOM-Acc is formed from one HOM- $RO_2$  (HOM- $RO_2+RO_2$ ) or potentially even two HOM-



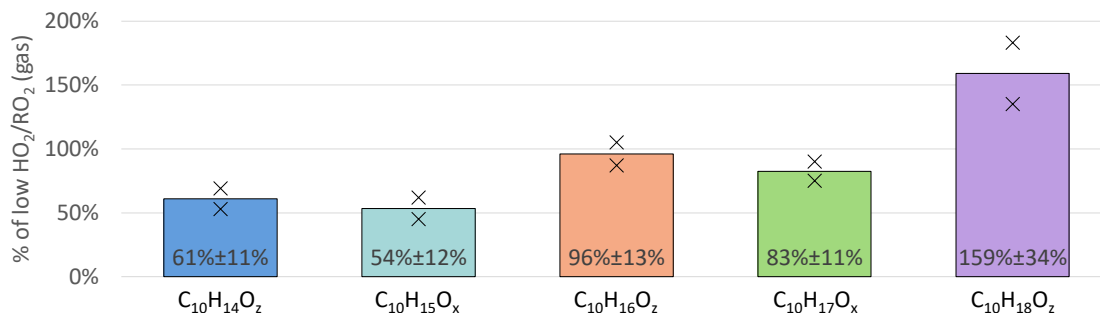
391 ~~RO<sub>2</sub>-(HOM-RO<sub>2</sub>+HOM-RO<sub>2</sub>).~~ Of course, the presence of HO<sub>2</sub> could reduce the alkoxy formation, and thus fragmentation  
 392 of HOM-RO<sub>2</sub>. This missing sink could lead to an additional HOM-Mon source compared to the low HO<sub>2</sub>/RO<sub>2</sub> case. However,  
 393 the distribution of the product classes at low and high HO<sub>2</sub>/RO<sub>2</sub> (Fig. 5) shows that contributions are shifted from HOM-Acc  
 394 to HOM-Mon, while the contribution of HOM-Frag remains constant. Each HOM-Acc is formed from one HOM-RO<sub>2</sub> (HOM-  
 395 RO<sub>2</sub>+RO<sub>2</sub>) or potentially even two HOM-RO<sub>2</sub> (HOM-RO<sub>2</sub>+HOM-RO<sub>2</sub>) and therefore each HOM-Acc not formed will lead to  
 396 at least one HOM-Mon.



397

398 **Figure 5: Average contribution of the closed shell product classes to overall HOM-product signal in the low and high HO<sub>2</sub>/RO<sub>2</sub> cases**  
 399 **(pure gas phase unseeded experiments).**

400 Further changes in the product distribution become evident when considering the individual HOM-Mon families as shown in  
 401 Fig. 6. The C<sub>10</sub>H<sub>15</sub>O<sub>x</sub> peroxy radical family and the related C<sub>10</sub>H<sub>14</sub>O<sub>z</sub> family (carbonyl compounds) show the strongest  
 402 suppression with a decrease of about 40 % at high HO<sub>2</sub>/RO<sub>2</sub>. For the C<sub>10</sub>H<sub>17</sub>O<sub>x</sub> peroxy radical family the suppression was less  
 403 pronounced with a 17 % reduction. In contrast, the C<sub>10</sub>H<sub>16</sub>O<sub>z</sub> family remained about the same while the C<sub>10</sub>H<sub>18</sub>O<sub>z</sub> family  
 404 showed a strong increase at high HO<sub>2</sub>/RO<sub>2</sub>.



405

406 **Figure 6: Overview of average, relative change in monomer families detected in NO<sub>3</sub>-CIMS between low and high HO<sub>2</sub>/RO<sub>2</sub> case**  
 407 **(both normalized to  $\alpha$ -pinene OH turnover) for pure gas phase unseeded experiments. Bars represent average of the two experiments,**  
 408 **markers represent individual experiments.**

409 The suppression of C<sub>10</sub>-HOM-RO<sub>2</sub> of only about 40 % compared to the reduction of overall [RO<sub>2</sub>] by ~70 % in the model  
410 calculations (for the modelled concentrations see supplement Sect. S4) shows that in many instances the autoxidation is too  
411 efficient to be out-competed by the RO<sub>2</sub>+HO<sub>2</sub> termination reaction, which is several times faster than RO<sub>2</sub>+RO<sub>2</sub> reactions.

412 Furthermore, the signal weighted O/C ratio of the monomer class does not change between low and high HO<sub>2</sub>/RO<sub>2</sub> (0.70±  
413 0.01). If the HO<sub>2</sub> termination would interrupt the autoxidation chain, a lower oxidation level would be expected at high  
414 HO<sub>2</sub>/RO<sub>2</sub>. The unchanged oxidation level and the suppression of HOM-Acc, indicate that the average autoxidation rate must  
415 be faster than  $k_{RO_2HO_2} \cdot [HO_2]$ , while the average accretion rate for  $k_{HOM-RO_2+RO_2} \cdot [RO_2]$  must be slower. In conclusion, the change  
416 in HO<sub>2</sub>/RO<sub>2</sub> should essentially impact the distribution of the HOM-RO<sub>2</sub> termination products.

### 417 3.24.2 Impact on HOM-RO<sub>2</sub>

418 C<sub>10</sub>-HOM-RO<sub>2</sub> are key to understand the changes in the HOM product distribution. Therefore, we will first discuss the changes  
419 in the HOM-RO<sub>2</sub> and then the changes in the closed shell products.

420 The C<sub>10</sub> peroxy radical class consists of the C<sub>10</sub>H<sub>15</sub>O<sub>x</sub> and C<sub>10</sub>H<sub>17</sub>O<sub>x</sub> families which were reduced to 54 % and 83 %,   
421 respectively when comparing the high and low HO<sub>2</sub>/RO<sub>2</sub> cases (**Fig. 6**, light blue and green bars). The observed reduction in  
422 C<sub>10</sub>-HOM-RO<sub>2</sub> is significantly smaller than the overall RO<sub>2</sub> concentration reduction predicted by the MCM model results  
423 (reduction to ~30 %). In the following paragraphs, we present a plausibility consideration to assess if these observed changes  
424 are consistent with our expectations from modelling results and reaction rates.

425 The change in the steady state concentration of a compound is always defined by the changes in its sources and sinks. The  
426 source of a HOM-RO<sub>2</sub> is the intramolecular reaction of a precursor RO<sub>2</sub> and thus the HOM-RO<sub>2</sub>'s source is reduced if the  
427 steady state concentration of the precursor RO<sub>2</sub> is reduced. However, assuming the source term of the precursor RO<sub>2</sub> is the  
428 same in low and high HO<sub>2</sub>/RO<sub>2</sub> (due to the constant  $\alpha$ -pinene OH turnover) and the precursor RO<sub>2</sub>'s sink term is dominated  
429 by the fast autoxidation in both cases, then the RO<sub>2</sub>'s steady state concentration would not be significantly changed. This  
430 consideration is only applicable for RO<sub>2</sub> where autoxidation dominates the sink term at low and high HO<sub>2</sub>/RO<sub>2</sub>. However, the  
431 unchanged oxidation level of the HOM-Mon indicates that once the autoxidation is initiated it out-competes the possible  
432 termination reactions.

433 In this case, the change in steady state concentration of the HOM-RO<sub>2</sub> will be defined by the changes in the sink terms. Owing  
434 to the faster reaction of RO<sub>2</sub>+HO<sub>2</sub> compared to RO<sub>2</sub>+RO<sub>2</sub> the chemical sink for all RO<sub>2</sub> including HOM-RO<sub>2</sub> with slower  
435 autoxidation rates increased, which leads to a reduction in the steady state concentration of RO<sub>2</sub> in general, despite holding the  
436 primary RO<sub>2</sub> source term constant.

437 For steady state conditions, we can estimate the expected effect of on the RO<sub>2</sub> ratio between high and low HO<sub>2</sub>/RO<sub>2</sub> on the RO<sub>2</sub>  
438 ratio conditions for those HOM-RO<sub>2</sub> with production directly linked to the primary production ( $k_{OH} \cdot [OH] \cdot [\alpha\text{-pinene}]$ ) with  
439 negligible further autoxidation. The necessary equations and assumptions can be found in supplement **Sect. S5S7**. We assume

440 the same primary production at low and high HO<sub>2</sub>/RO<sub>2</sub> and that the reaction with HO<sub>2</sub>, the reaction with RO<sub>2</sub> and the wall loss  
441 are the only significant loss pathways. At high HO<sub>2</sub>/RO<sub>2</sub>, a reduction to 80 % is expected if the chosen bulk rate coefficient  
442 constants are used ( $k_{\text{RO}_2\text{HO}_2} = 1.85 = 2.46 \cdot 10^{-11} \text{ cm}^3 \cdot \text{s}^{-1}$  at 20 °C (Jenkin et al., 1997; Saunders et al., 2003)) is 5 times  
443 faster than  $k_{\text{RO}_2\text{RO}_2}$  (leading to  $k_{\text{RO}_2\text{RO}_2} = 3.7 \cdot 10^{-12} \text{ cm}^3 \cdot \text{s}^{-1}$ ). A reduction to 60 % is expected if  $k_{\text{RO}_2\text{HO}_2}$  is around 7  
444 times faster than  $k_{\text{RO}_2\text{RO}_2}$  ( $k_{\text{RO}_2\text{RO}_2} = 3.3 \cdot 10^{-12} \text{ cm}^3 \cdot \text{s}^{-1}$ ). These reductions are in the range of what is observed for the C<sub>10</sub>-HOM-RO<sub>2</sub>. Of  
445 course, the approach of using generalized bulk rate constants is limited, but the resulting values for  $k_{\text{RO}_2\text{RO}_2}$  were clearly within  
446 the range of rate coefficients expected for HOM-RO<sub>2</sub>+RO<sub>2</sub> reactions (Roldin et al., 2019) showing that the increased chemical  
447 sink is a plausible explanation for our observations.

448 The C<sub>10</sub>H<sub>15</sub>O<sub>x</sub> family is on average reduced by around 30 % more than the C<sub>10</sub>H<sub>17</sub>O<sub>x</sub> family (see **Fig. 6**). C<sub>10</sub>H<sub>15</sub>O<sub>x</sub> peroxy  
449 radicals are either formed by sequential oxidation of α-pinene, e.g. from oxidation products like pinonaldehyde, or directly  
450 from α-pinene via the H-abstraction pathway (Shen et al., 2022). Formation of pinonaldehyde and, even more so HOM  
451 formation via the H-abstraction channel, involve alkoxy steps. However, alkoxy radicals should be reduced at high HO<sub>2</sub>/RO<sub>2</sub>  
452 since they are mainly formed by RO<sub>2</sub>+RO<sub>2</sub> reactions in the absence of NO<sub>x</sub>. Thus, missing source terms add to the increased  
453 chemical sink by HO<sub>2</sub> for C<sub>10</sub>H<sub>15</sub>O<sub>x</sub> peroxy radicals.

454 Amine CIMS measurements enabled detection of the formula composition C<sub>10</sub>H<sub>16</sub>O<sub>2</sub> (e.g. pinonaldehyde). C<sub>10</sub>H<sub>16</sub>O<sub>2</sub> was  
455 reduced on average to 71% ± 1 % at high HO<sub>2</sub>/RO<sub>2</sub> compared to low HO<sub>2</sub>/RO<sub>2</sub>. This supports that a fraction of the C<sub>10</sub>H<sub>15</sub>O<sub>x</sub>  
456 radical decrease at high HO<sub>2</sub>/RO<sub>2</sub> arose from suppression of C<sub>10</sub>H<sub>16</sub>O<sub>2</sub> first generation products. In addition, a further  
457 suppression of HOM formation via the H-abstraction channel is likely. It should be noted that the reduction of C<sub>10</sub>H<sub>16</sub>O<sub>2</sub> is  
458 smaller than that expected by the MCM model results. Modelling results can be found in supplement Sect. S4. This might  
459 indicate that HO<sub>2</sub> can also enable alkoxy radical steps to a certain degree as summarized by Jenkin et al. (2019) and postulated  
460 by e.g. Eddingsaas et al. (2012) as a source of pinonaldehyde in HO<sub>2</sub> dominated systems.

461 According to the model calculations the pseudo first order rate coefficient  $k_{\text{RO}_2\text{HO}_2}[\text{HO}_2]$  is expected to be about 0.03 s<sup>-1</sup> for  
462 the RO<sub>2</sub>+HO<sub>2</sub> reaction at high HO<sub>2</sub>/RO<sub>2</sub>. Consequently, only such HOM-RO<sub>2</sub> with autoxidation rates of ≤0.03 s<sup>-1</sup> will be  
463 significantly lost by reaction with HO<sub>2</sub> at the higher HO<sub>2</sub> concentrations. However, typical isomerization rates of peroxy  
464 radicals in autoxidation are of the order of 0.1 s<sup>-1</sup> and many are faster (Piletic and Kleindienst, 2022; Berndt, 2021). Therefore,  
465 reduction in a HOM-RO<sub>2</sub> is only expected when the faster termination rate of  $k_{\text{RO}_2\text{HO}_2}[\text{HO}_2]$  can compete with the autoxidation  
466 rate, i. e. when the autoxidation slows as the degree of oxidation increases on the specific HOM-RO<sub>2</sub> However, typical  
467 isomerization rates of peroxy radicals in autoxidation are of the order of 0.1 s<sup>-1</sup> and many are faster (Piletic and Kleindienst,  
468 2022; Berndt, 2021). Therefore, reduction in a HOM-RO<sub>2</sub> is only expected when the faster termination rate of  $k_{\text{RO}_2\text{HO}_2}[\text{HO}_2]$   
469 can compete with the autoxidation rate, i. e. when the autoxidation slows as the degree of oxidation increases on the specific  
470 HOM-RO<sub>2</sub>. This consideration shows that the smaller reduction in HOM-RO<sub>2</sub> compared to the lower oxidized RO<sub>2</sub> in the  
471 model is compatible with fast autoxidation reactions that are missing in the MCM.

472 The increase in chemical sink strength by going from RO<sub>2</sub> termination to HO<sub>2</sub> termination is the main expected reason for the  
473 decrease in C<sub>10</sub>H<sub>17</sub>O<sub>x</sub>. As discussed, the C<sub>10</sub>H<sub>15</sub>O<sub>x</sub> family is subject to an additional decrease in the precursors due to the alkoxy  
474 steps necessary in the formation pathway. Since C<sub>10</sub>H<sub>15</sub>O<sub>x</sub> were the main contributors to the C<sub>10</sub>-HOM-RO<sub>2</sub> class their stronger  
475 reduction is reflected in the overall reduction of C<sub>10</sub>-HOM-RO<sub>2</sub>.

#### 476 [3.2.14.2.1](#) Contribution of C<sub>10</sub>H<sub>15</sub>O<sub>x</sub> and C<sub>10</sub>H<sub>17</sub>O<sub>x</sub> families to HOM-RO<sub>2</sub>

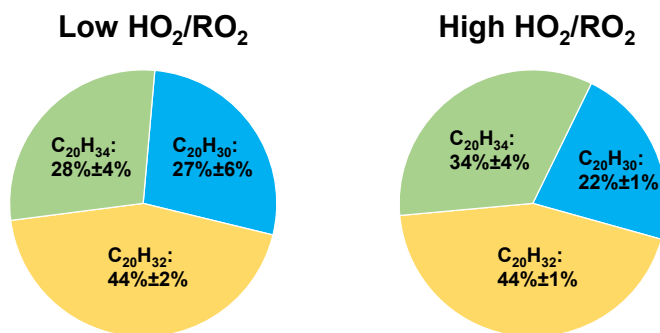
477 In the unseeded, pure gas phase experiments, the contribution of the C<sub>10</sub>H<sub>17</sub>O<sub>x</sub> family to the C<sub>10</sub>-HOM-RO<sub>2</sub> class is 23 % ± 2 %  
478 on average in the low HO<sub>2</sub>/RO<sub>2</sub> case. In the high HO<sub>2</sub>/RO<sub>2</sub> case the contribution increases to 31 % ± 4 % on average. As  
479 discussed above the suggested pathways to C<sub>10</sub>H<sub>15</sub>O<sub>x</sub> HOM-RO<sub>2</sub> may be additionally suppressed due to a decrease of alkoxy  
480 steps at high HO<sub>2</sub>/RO<sub>2</sub> reducing the entry channel into C<sub>10</sub>H<sub>15</sub>O<sub>x</sub> HOM-RO<sub>2</sub>.

481 Nevertheless, the contribution of C<sub>10</sub>H<sub>15</sub>O<sub>x</sub> is substantial in both experiment stages. Kang (2021) and Shen et al. (2022) reported  
482 that, in the photooxidation of α-pinene, the HOM-RO<sub>2</sub> detected by NO<sub>3</sub>-CIMS are dominated by the C<sub>10</sub>H<sub>15</sub>O<sub>x</sub> family, while  
483 C<sub>10</sub>H<sub>17</sub>O<sub>x</sub> formation is the main expected OH reaction pathway described in literature (Berndt, 2021; Berndt et al., 2016; Xu  
484 et al., 2019).

485 This hints towards an effective pathway to HOM via C<sub>10</sub>H<sub>15</sub>O<sub>x</sub>. A reason may be the fast opening of both carbon-rings in the  
486 bicyclic α-pinene (Shen et al., 2022), or a four-ring opening in pinonaldehyde or similar compounds, for easy autoxidation.  
487 From our observations increasing the HO<sub>2</sub>/RO<sub>2</sub> ratio does increase the relative importance of the C<sub>10</sub>H<sub>17</sub>O<sub>x</sub> family, but the  
488 change is less than 10 % in contribution.

489 Contribution of the two peroxy radical families to the HOM formation is also reflected in the composition of C<sub>20</sub> HOM-Acc.  
490 **Figure 7** shows the average contributions of the C<sub>20</sub>H<sub>30</sub>O<sub>z</sub>, C<sub>20</sub>H<sub>32</sub>O<sub>z</sub>, and C<sub>20</sub>H<sub>34</sub>O<sub>z</sub> families in the low and high HO<sub>2</sub>/RO<sub>2</sub>  
491 cases. Although the absolute amount of HOM-Acc was suppressed by 60 % the family distribution was similar, C<sub>20</sub>H<sub>32</sub>O<sub>z</sub>  
492 dominated, while C<sub>20</sub>H<sub>30</sub>O<sub>z</sub> was lowest. C<sub>20</sub>H<sub>30</sub>O<sub>z</sub> is formed from two members of the C<sub>10</sub>H<sub>15</sub>O<sub>x</sub> family, while C<sub>20</sub>H<sub>34</sub>O<sub>z</sub> is  
493 formed by two members of the C<sub>10</sub>H<sub>17</sub>O<sub>x</sub> family. C<sub>20</sub>H<sub>32</sub>O<sub>z</sub> is then a combination of a C<sub>10</sub>H<sub>15</sub>O<sub>x</sub>-RO<sub>2</sub> and C<sub>10</sub>H<sub>17</sub>O<sub>x</sub>-RO<sub>2</sub>.

494 Families that require one or two C<sub>10</sub>H<sub>17</sub>O<sub>x</sub> peroxy radicals for their formation have a higher contribution than the C<sub>10</sub>H<sub>17</sub>O<sub>x</sub>  
495 family's contribution to C<sub>10</sub>-HOM-RO<sub>2</sub>. Here, it is important to note that not only HOM-RO<sub>2</sub> can participate in HOM-Acc  
496 formation, but also traditional, less oxidized RO<sub>2</sub> radicals (Berndt et al., 2018; Pullinen et al., 2020; McFiggans et al., 2019),  
497 which are not detectable by NO<sub>3</sub><sup>-</sup>-CIMS. However, more oxidized peroxy radicals exhibit faster accretion rates (Berndt et al.,  
498 2018).



499

500 **Figure 7: Average contribution of the C<sub>20</sub>H<sub>30</sub>O<sub>z</sub>, C<sub>20</sub>H<sub>32</sub>O<sub>z</sub>, and C<sub>20</sub>H<sub>34</sub>O<sub>z</sub> family to the C<sub>20</sub> HOM-Acc group signal in the low and**  
 501 **high HO<sub>2</sub>/RO<sub>2</sub> cases (pure gas phase unseeded experiments). Not pictured is C<sub>20</sub>H<sub>28</sub>O<sub>z</sub> due to its negligible signal (contribution**  
 502 **~1 %).**

503 The large contributions of C<sub>20</sub>H<sub>32</sub>O<sub>z</sub> and C<sub>20</sub>H<sub>34</sub>O<sub>z</sub> thus clearly show the general importance of the C<sub>10</sub>H<sub>17</sub>O<sub>x</sub> peroxy radicals.

504 The largest fraction, the C<sub>20</sub>H<sub>32</sub>O<sub>z</sub> family ~~reflects the importance of HOM-C<sub>10</sub>H<sub>15</sub>O<sub>x</sub> and the high abundance of lower oxidized~~  
 505 ~~C<sub>10</sub>H<sub>17</sub>O<sub>x</sub> peroxy radicals. indicates the importance of HOM-C<sub>10</sub>H<sub>15</sub>O<sub>x</sub> and a high abundance of lower oxidized C<sub>10</sub>H<sub>17</sub>O<sub>x</sub>~~  
 506 ~~peroxy radicals. Lower oxidized C<sub>10</sub>H<sub>17</sub>O<sub>x</sub>-RO<sub>2</sub> were recently measured by Berndt (2021).~~ The fraction of C<sub>20</sub>H<sub>34</sub>O<sub>z</sub> is smaller  
 507 because their formation requires HOM-C<sub>10</sub>H<sub>17</sub>O<sub>x</sub> radicals which are less abundant compared to HOM-C<sub>10</sub>H<sub>15</sub>O<sub>x</sub>, while the  
 508 small fraction of C<sub>20</sub>H<sub>30</sub>O<sub>z</sub> indicates that, despite the importance of HOM-C<sub>10</sub>H<sub>15</sub>O<sub>x</sub>, lower oxidized C<sub>10</sub>H<sub>15</sub>O<sub>x</sub> are less  
 509 important.

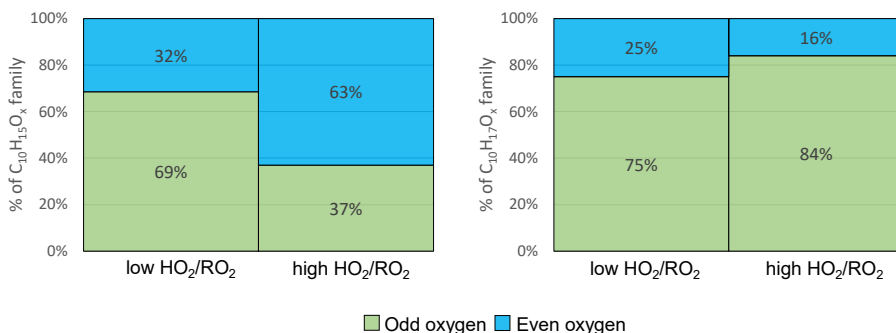
510 These results indicate the importance of mixed HOM-Acc formation by cross reactions of HOM-RO<sub>2</sub> and a lower oxidized  
 511 RO<sub>2</sub>. The importance of mixed HOM-Acc is supported by the relatively small fractions of HOM-Acc products with very high  
 512 oxygen numbers, which more likely stem from HOM-RO<sub>2</sub>+HOM-RO<sub>2</sub>. For example, C<sub>20</sub>-HOM-Acc with 12 or more oxygen  
 513 atoms contribute only around 30 % (low HO<sub>2</sub>/RO<sub>2</sub>: 26 % ±4 %, high HO<sub>2</sub>/RO<sub>2</sub>: 31 % ±2 %) of the signal in the product group.

514 Although the effect of the changed HO<sub>2</sub>/RO<sub>2</sub> ratio is small, a tendency to higher C<sub>20</sub>H<sub>34</sub>O<sub>z</sub> contribution was observed. This is  
 515 consistent with the observation of a slightly higher C<sub>10</sub>H<sub>17</sub>O<sub>x</sub> contribution to the C<sub>10</sub>-HOM RO<sub>2</sub>. The stronger suppression of  
 516 the C<sub>10</sub>H<sub>15</sub>O<sub>x</sub> family at high HO<sub>2</sub>/RO<sub>2</sub> is the first indication for, and can be explained by, a reduction in the alkoxy radical  
 517 formation.

### 518 3.2.24.2.2 **Impact on HOM-Alkoxy radical formation**

519 Alkoxy radicals (RO) are the second important radical type in the oxidation chain of α-pinene. RO cannot be detected directly  
 520 as they are highly unstable and thus have very low concentrations. However, as explained in **Sect. Fehler! Verweisquelle**  
 521 ~~konnte nicht gefunden werden-2.1~~ the parity change in the HOM-RO<sub>2</sub> families can be used as a diagnosis tool for the abundance  
 522 of alkoxy steps (Kang, 2021). A second indicator for alkoxy steps is the abundance of HOM products with less than 10 C-  
 523 atoms.

524 **Figure 8** shows the average contribution of  $C_{10}H_{15}O_x$  and  $C_{10}H_{17}O_x$  with an even and odd number of oxygens at low and high  
 525  $HO_2/RO_2$ .  $C_{10}H_{15}O_x$  radicals with an even number of oxygens contribute on average 32 % at low  $HO_2/RO_2$ . For  $C_{10}H_{15}O_x$ , the  
 526 autoxidation chain is expected to start from an even number of oxygen either from  $C_{10}H_{15}O_4$  (pinonaldehyde-like) (MCM  
 527 v3.3.1 (Jenkin et al., 1997; Saunders et al., 2003) or from  $C_{10}H_{15}O_2$  ( $C_{10}H_{16}$  H-abstraction) (Berndt, 2021; Shen et al., 2022).  
 528 Therefore, without the involvement of an alkoxy step, the parity of the oxygen number in the observed  $C_{10}H_{15}O_x$  HOM- $RO_2$   
 529 is expected to be even. Due to the average contribution of  $C_{10}H_{15}O_{\text{odd}}$  of 69 % we conclude that at least one alkoxy step (or  
 530 any odd number of alkoxy steps) must have taken place in most of the cases at low  $HO_2/RO_2$ .



531

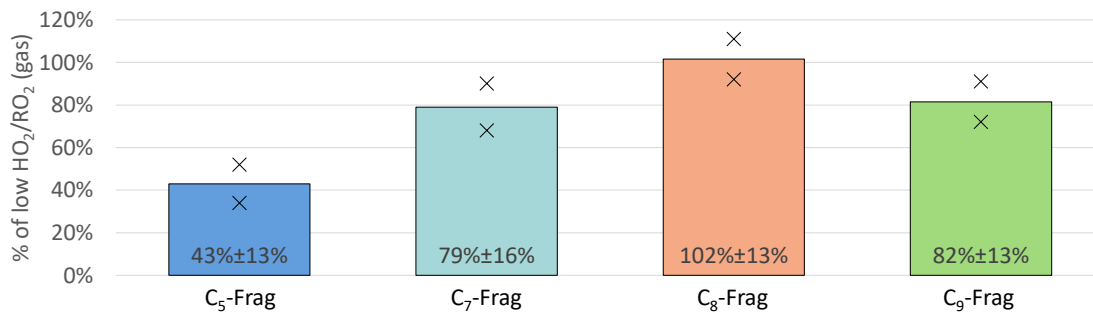
532 **Figure 8: Average contribution of  $O_{\text{odd}}$  and  $O_{\text{even}}$  to the HOM- $RO_2$  families  $C_{10}H_{15}O_x$  (left) and  $C_{10}H_{17}O_x$  (right) signal in the low  
 533 and high  $HO_2/RO_2$  cases (pure gas phase unseeded experiments).**

534 At high  $HO_2/RO_2$   $C_{10}H_{15}O_{\text{even}}$  contributed 63 % and the  $C_{10}H_{15}O_{\text{odd}}$  contribution was reduced to 37 %. This demonstrates a  
 535 change in the number of alkoxy steps along the formation pathway of the observed HOM- $RO_2$  radicals. The increased  
 536 contribution of  $C_{10}H_{15}O_{\text{even}}$  at high  $HO_2/RO_2$  lets us infer an even number of alkoxy steps as more common (0,2,4...). In the  
 537 simplest case 1 ~~or 2~~ alkoxy step ~~taketakes~~ place at low  $HO_2/RO_2$  due to HOM-RO formation from HOM- $RO_2+RO_2$  reactions,  
 538 while no ~~or 1~~ alkoxy step ~~taketakes~~ place at high  $HO_2/RO_2$ , because HOM- $RO_2+HO_2$  produces none or less HOM-RO than  
 539 HOM- $RO_2+RO_2$ .

540 For  $C_{10}H_{17}O_x$  the entry channel into autoxidation is  $C_{10}H_{17}O_3$  with an odd number of oxygen atoms. Therefore, in autoxidation  
 541 without alkoxy steps the oxygen parity is expected to be odd. At low  $HO_2/RO_2$   $C_{10}H_{17}O_{\text{odd}}$  species contribute 75 % to the total  
 542  $C_{10}H_{17}O_x$  signal indicating that either none or an even number (2,4,...) of alkoxy steps occurred. At high  $HO_2/RO_2$  the odd  
 543 contribution increases to 84 % (see **Fig. 8**). This result could indicate a low occurrence of alkoxy steps even at low  $HO_2/RO_2$ ,  
 544 with a further decrease of alkoxy formation at high  $HO_2/RO_2$ . However, the observed shift is minor.

545 In any case the different responses of the  $C_{10}H_{15}O_x$  and  $C_{10}H_{17}O_x$  families to the reduction of HOM- $RO_2$  formation from HOM-  
 546  $RO_2+RO_2$  at high  $HO_2/RO_2$  indicate that there could be fundamental differences in the autoxidation chains of  $C_{10}H_{15}O_x$  and  
 547  $C_{10}H_{17}O_x$  (or the limit of the parity analysis). The parity analysis indicates a decrease in alkoxy steps at high  $HO_2/RO_2$ , but it  
 548 cannot be directly inferred with certainty. However, decrease in alkoxy steps at high  $HO_2/RO_2$  is supported by the observation  
 549 of changes in HOM-Frag products.

550 On average the sum of all HOM-Frag products (detected compounds with  $5 \leq C < 10$  by  $\text{NO}_3^-$ -CIMS) showed a reduction of  
 551 around 20 % (~~pure gas phase unseeded~~ experiments, see **Fig. 4**). Further trends become recognizable when separating the  
 552 species according to their carbon number. **Figure 9** shows the  $\text{C}_5$ ,  $\text{C}_7$ ,  $\text{C}_8$ , and  $\text{C}_9$  HOM-Frag at high  $\text{HO}_2/\text{RO}_2$  compared to the  
 553 low  $\text{HO}_2/\text{RO}_2$  case, normalized to the  $\alpha$ -pinene OH turnover. The fragment group with  $\text{C}_6$  compounds is not included, as it  
 554 contributed less than 5 % of the fragment signal and contained few detected compounds.



555

556 **Figure 9: Overview of average, relative change in  $\text{C}_5$ ,  $\text{C}_7$ ,  $\text{C}_8$ ,  $\text{C}_9$  fragment groups detected in  $\text{NO}_3^-$ -CIMS between high and low**  
 557  **$\text{HO}_2/\text{RO}_2$  case (both normalized to  $\alpha$ -pinene OH turnover) for ~~pure gas phase unseeded~~ experiments. Bars represent average of the**  
 558 **two experiments, markers represent individual experiments.**

559 **Figure 9** shows a significant reduction in HOM-Frag with shorter carbon chain length:  $\text{C}_5$  HOM-Frag are reduced by around  
 560 60 % compared to the low  $\text{HO}_2/\text{RO}_2$  case. If we assume that the fragmentation of  $\text{C}_{10}$  compounds happens in consecutive steps  
 561 via scission of HOM-RO radicals (analogously to the MCM), this observation is in accord with decreasing importance of  
 562 alkoxy radical formation at high  $\text{HO}_2/\text{RO}_2$ .

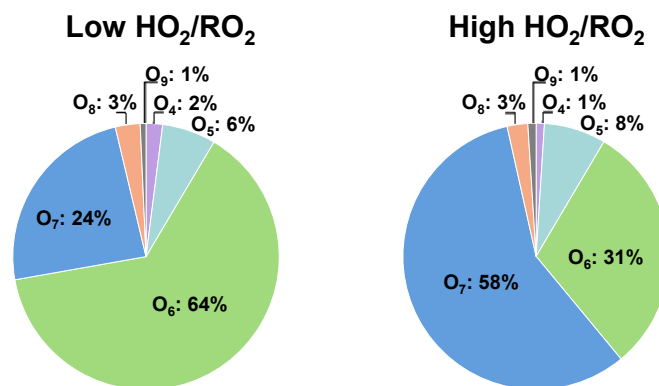
563 Overall, all observations indicate strong involvement of RO in HOM formation as well as a reduced, but still significant,  
 564 involvement of RO at high  $\text{HO}_2/\text{RO}_2$ , when  $\text{HO}_2$  chemistry dominates: This is supported by the change of the oxygen parity  
 565 in  $\text{C}_{10}$ -HOM- $\text{RO}_2$ , and the decrease of fragmentation products, especially with lower carbon number, as well as the only  
 566 moderate reduction in the observed  $\text{C}_{10}\text{H}_{16}\text{O}_2$  product (pinonaldehyde) and the still substantial importance of the  $\text{C}_{10}\text{H}_{15}\text{O}_x$   
 567 HOM- $\text{RO}_2$  family at high  $\text{HO}_2/\text{RO}_2$ .

### 568 **3.34.3 Impact on carbonyl and hydroperoxide formation**

569 Increased  $\text{HO}_2/\text{RO}_2$  should shift the product distribution by reduction of alcohol and carbonyl compounds from the so-called  
 570 molecular channel in the  $\text{RO}_2+\text{RO}_2$  reaction (see reaction (**R3**)), in favor of hydroperoxide formation from  $\text{RO}_2+\text{HO}_2$   
 571 termination (reaction (**RI**)). This effect can be best observed in the  $\text{C}_{10}\text{H}_{18}\text{O}_z$  family, which contains the hydroperoxide and  
 572 alcohol termination products arising from  $\text{C}_{10}\text{H}_{17}\text{O}_x$ .  $\text{C}_{10}\text{H}_{18}\text{O}_z$  significantly increased to on average 159 % (see **Fig. 6**). This  
 573 supports an increased hydroperoxide formation, however, with some uncertainty due to the alcohol termination products from  
 574  $\text{C}_{10}\text{H}_{17}\text{O}_x$  (by reaction with  $\text{RO}_2$ ). To elucidate this further the contribution of individual species to the  $\text{C}_{10}\text{H}_{18}\text{O}_z$  family was  
 575 examined.

576 Formation of an alcohol via the molecular path (reaction (**R3**)) leads to the loss of one oxygen atom compared to the precursor  
 577  $C_{10}H_{17}O_x$  radical, while in the hydroperoxide formation (reaction (**RI**)) the oxygen number remains the same. The most  
 578 abundant member of the  $C_{10}H_{17}O_x$  family was  $C_{10}H_{17}O_7$  with a contribution of 72 %  $\pm$  6 % at low  $HO_2/RO_2$ , and a contribution  
 579 of 82 %  $\pm$  1 % at high  $HO_2/RO_2$ .  $C_{10}H_{17}O_7$  terminates to  $C_{10}H_{18}O_z$  products either as an alcohol with sum formula  $C_{10}H_{18}O_6$ ,  
 580 or as a hydroperoxide with sum formula  $C_{10}H_{18}O_7$ . These products have additional sources from  $C_{10}H_{17}O_6$  and  $C_{10}H_{17}O_8$  but  
 581 due to the dominant contribution of  $C_{10}H_{17}O_7$  to the  $C_{10}H_{17}O_x$  family we expect any other production channels to be of minor  
 582 importance.

583 **Figure 10** shows the HOM product distribution within the  $C_{10}H_{18}O_z$  family at low and high  $HO_2/RO_2$ . The sum of the  $O_6$  and  
 584  $O_7$  product did not change significantly in the two regimes (about 88 %), showing that these are the major products, and  
 585 agreeing well with the observation of  $C_{10}H_{17}O_7$  being the major  $C_{10}H_{17}O_x$  HOM- $RO_2$ . At low  $HO_2/RO_2$  the  $O_6$  product has a  
 586 larger contribution of 64 %  $\pm$  8 %, while at high  $HO_2/RO_2$  ~30% of signal is shifted to the  $O_7$  product. This shows that the  
 587 increase in the  $C_{10}H_{18}O_z$  is matched with an increase of hydroperoxide formation.



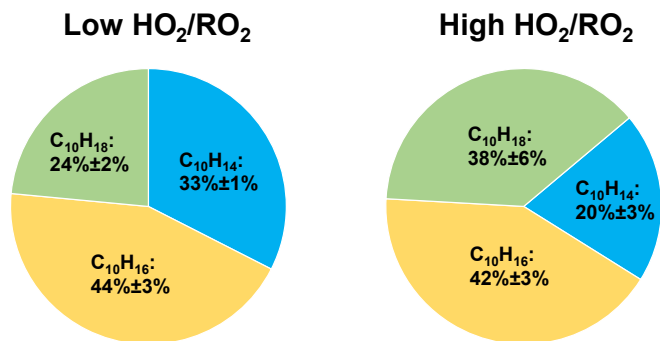
588  
 589 **Figure 10: Average contribution of the individual compounds to the  $C_{10}H_{18}O_z$  family signal at low and high  $HO_2/RO_2$  (pure-gas**  
 590 **phaseunseeded experiments).**

591 An indicator for carbonyl formation is the  $C_{10}H_{14}O_z$  family as it only contains the carbonyl products arising from  
 592  $C_{10}H_{15}O_x-RO_2$ . The  $C_{10}H_{14}O_z$  family was reduced on average to 61 % at high  $HO_2/RO_2$ , however this decrease matches the  
 593 decrease in the  $C_{10}H_{15}O_x$  precursor family. If the reaction of a  $C_{10}H_{15}O_x$ -HOM- $RO_2$  with a second  $RO_2$  were the main formation  
 594 pathway for  $C_{10}H_{14}O_z$  a stronger reduction would be expected as both precursor species were decreased significantly. Instead,  
 595 it appears that  $C_{10}H_{14}O_z$  is mainly impacted by the decrease in  $C_{10}H_{15}O_x$  as their reductions are similar. A possible explanation  
 596 could be that intramolecular termination is a major reaction pathway for  $C_{10}H_{15}O_x-RO_2$ , forming  $C_{10}H_{14}O_x$ -carbonyls.  
 597 Intramolecular termination of the autoxidation chain has been discussed in the literature for different VOCs (Shen et al., 2021;  
 598 Guo et al., 2022), Rissanen et al. (2014) discussed the possible importance of the unimolecular termination via an H-shift,  
 599 followed by formation of a carbonyl functional group and OH loss in the autoxidation chain of cyclohexene. **Piletic and**  
 600 **Kleindienst (2022)****Piletic and Kleindienst (2022)** calculated fast reaction rate constants in the range of 1-30  $s^{-1}$  for such



601 intramolecular termination reactions to carbonyls for some  $C_{10}H_{17}O_5$  in the  $\alpha$ -pinene photooxidation, indicating that this  
602 pathway could also be significant for  $C_{10}H_{15}O_x$ . However, more investigation is necessary.

603 The overall contributions of the  $C_{10}H_{14}O_z$ ,  $C_{10}H_{16}O_z$ , and  $C_{10}H_{18}O_z$  families to the HOM-Mon class at high  $HO_2/RO_2$  are shifted  
604 as shown in **Fig. 11**.



605

606 **Figure 11: Average contribution of the  $C_{10}H_{14}O_z$ ,  $C_{10}H_{16}O_z$ , and  $C_{10}H_{18}O_z$  family to the monomer class signal at low and high**  
607  **$HO_2/RO_2$  (pure-gas-phase unseeded experiments).**

608 The contribution of  $C_{10}H_{16}O_z$  is largest and remains similar in both cases, matching the already shown unchanged signal level  
609 in **Fig. 6**. This is the case because the  $C_{10}H_{16}O_z$  family contains the alcohols from  $C_{10}H_{15}O_x+RO_2$ , carbonyls from  
610  $C_{10}H_{17}O_x+RO_2$  and hydroperoxides from  $C_{10}H_{15}O_x+HO_2$  (see **Fig. 1**). A separation of the effects of enhanced  $HO_2$  on this  
611 monomer family is difficult, as for the case where  $RO_2$  termination dominates vs. the case where  $HO_2$  termination dominates,  
612 the loss of carbonyls and alcohols is partially compensated by the gain of hydroperoxides. A strong gain in hydroperoxides is  
613 clearly reflected in the strong increase of  $C_{10}H_{18}O_z$  at high  $HO_2/RO_2$ .

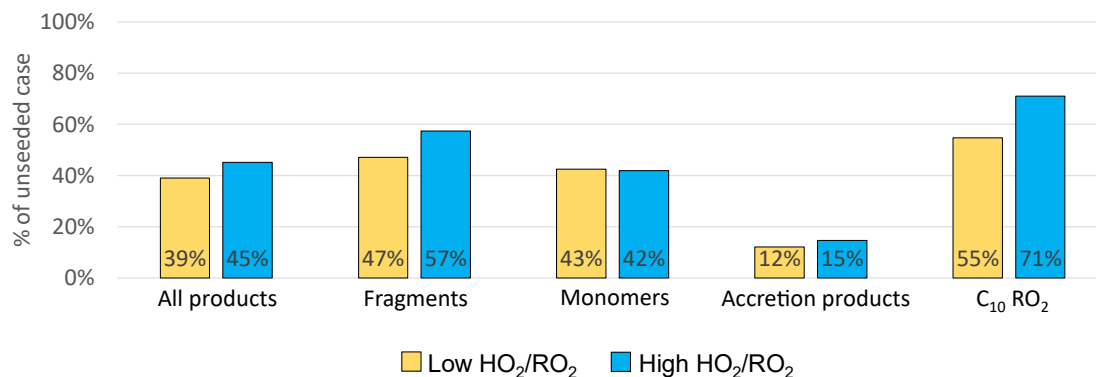
614 Inspection of the  $C_{10}H_{14}O_z$  and  $C_{10}H_{18}O_z$  families shows that ~13 % of the contribution by  $C_{10}H_{14}O_z$  are lost (carbonyls, 33 %  
615 at low  $HO_2/RO_2$ ) and are present instead as  $C_{10}H_{18}O_z$  (hydroperoxides), giving  $C_{10}H_{18}O_z$  a contribution of 38 % at high  
616  $HO_2/RO_2$ .

#### 617 **3.44.4 Impact on condensable organic mass**

618 In the previous sections we demonstrated a shift of the product distribution by the shift from low to high  $HO_2/RO_2$  conditions.  
619 We also showed that the changes could be rationalized by generic mechanistic considerations. We added  $(NH_4)_2SO_4$  seed  
620 aerosol in two experiments to determine how the shift in the product distribution affects the condensable organic mass by  
621 determining the fraction which remained in the gas-phase after seeding.

622 **Figure 12** shows the fraction remaining for the sum of all products as well as for the individual product classes for the high  
623 and the low  $HO_2/RO_2$  case. In both cases a significant reduction of products in the gas phase was observed with seed present.  
624 Overall, the sum of all products was reduced by around 60 %, with a slightly higher reduction in the low  $HO_2/RO_2$  case. This  
625 can be attributed to the larger importance of HOM-Acc in the low  $HO_2/RO_2$  case, as well as to a 10 % lower reduction of the

626 HOM-Frag in the high HO<sub>2</sub>/RO<sub>2</sub> case. In both cases a reduction of the HOM-RO<sub>2</sub> is observed, which indicates that the provided  
627 particle sink could have affected HOM formation chemistry, however only moderately.



628

629 **Figure 12: Overview of average, relative change in product classes signal between gas phase only and seeded system. Blue shows the**  
630 **high HO<sub>2</sub>/RO<sub>2</sub> case, yellow the low HO<sub>2</sub>/RO<sub>2</sub> case. (All are normalized to  $\alpha$ -pinene OH turnover, Exp2 experiment)**

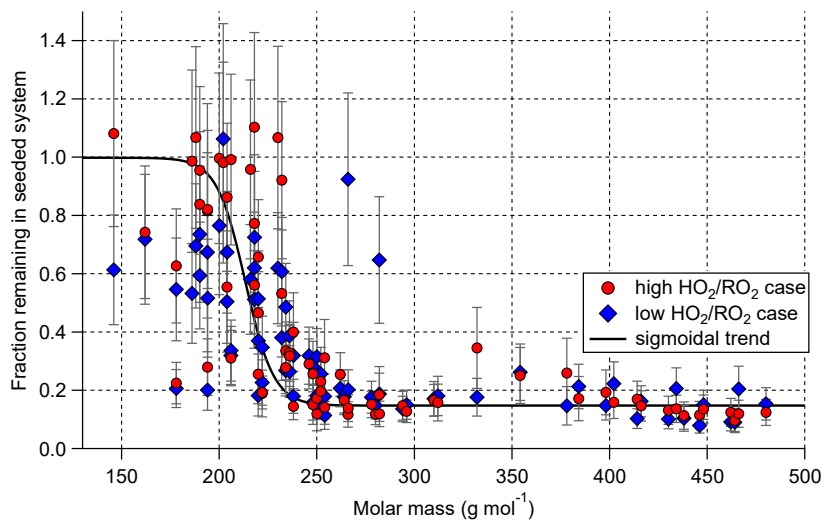
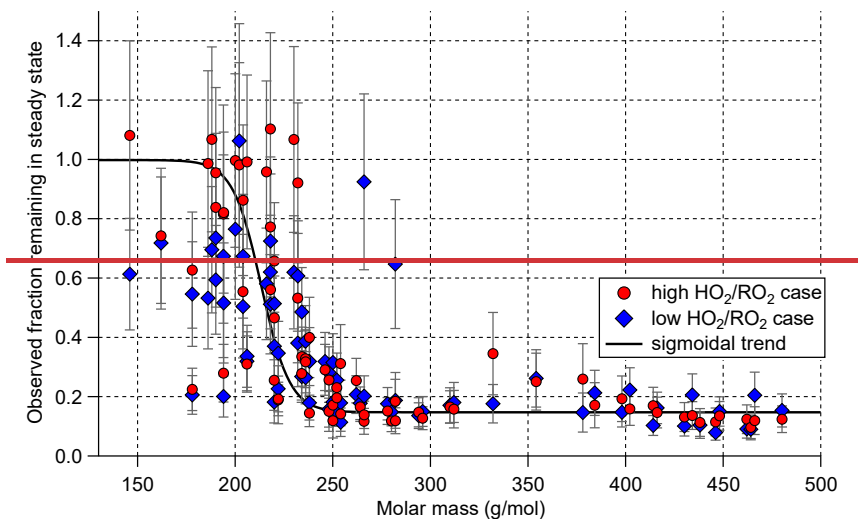
631 The total organic particulate mass was determined by AMS measurements and was 2.0  $\mu\text{g m}^{-3}$  and 3.4  $\mu\text{g m}^{-3}$  at high and low  
632 HO<sub>2</sub>/RO<sub>2</sub> in the experiment (Exp2) displayed in **Fig. 12**. A reduction of condensed organic mass to 73 % $\pm$ 3 % at high HO<sub>2</sub>/RO<sub>2</sub>  
633 (orange bar in **Fig. 14**) was observed on average. Since non-seeded and seeded experiments were conducted at otherwise the  
634 same conditions and we did not observe significant new particle formation, the gas-phase compositions can be directly  
635 compared. Therefore, we conclude that the shift in the product distribution led to a reduction of condensable material at the  
636 same  $\alpha$ -pinene turnover with OH (and O<sub>3</sub>).

637 We calculated the wall loss corrected SOA yields with the corrected SOA mass as shown in **Eq. (4)** and as described by  
638 Sarrafzadeh et al. (2016). To this end we used C<sub>10</sub>H<sub>16</sub>O<sub>7</sub> as the lead HOM compound. In the two experiments with seed present  
639 (Exp2.1 and Exp3) we had SOA yields of 7.3 % and 10.0 % at high HO<sub>2</sub>/RO<sub>2</sub> and 10.0 % and 12.8 % at low HO<sub>2</sub>/RO<sub>2</sub>. The  
640 difference in the SOA yields between experiments can be explained by the slightly different OH concentrations and subsequent  
641 difference in contribution by photooxidation (see **Table 1**). Overall, our yields are in the lower range in comparison with the  
642 SOA yields reported by McFiggans et al. (2019) for the  $\alpha$ -pinene photooxidation. However, our experiments were also  
643 performed at 5 °C higher temperature (20 °C) compared to 15 °C in McFiggans et al. (2019)). The SOA yields show an absolute  
644 reduction of ~3 % at high HO<sub>2</sub>/RO<sub>2</sub> compared to low HO<sub>2</sub>/RO<sub>2</sub> (relative a reduction of about 30 %). A reduction of the SOA  
645 yield of  $\alpha$ -pinene by addition of CO was described before by McFiggans et al. (2019), however, there the  $\alpha$ -pinene OH turnover  
646 was not held constant.

647 The change from low to high HO<sub>2</sub>/RO<sub>2</sub> regime favored termination reactions to protic termination groups, as we observed less  
648 carbonyl compounds and more hydroperoxides. This could overall shift the product distribution to products with lower vapor  
649 pressures and favor SOA formation, since protic groups can act as hydrogen bond donors as well as hydrogen bond acceptors.  
650 (asAs exemplified by the comparison of ethanol (boiling point (b.p) 78 °C) and ethane hydroperoxide (b.p. 93-97 °C) with

651 acetaldehyde (b.p. 20 °C) (Richter et al., 1955)). However, the effect of the termination group should be small for HOM as  
652 they likely contain multiple hydroperoxide groups (compare Pullinen et al. (2020)). The reduction in HOM-Acc is expected to  
653 decrease the condensable mass, since the HOM-Acc scavenge non-HOM-RO<sub>2</sub>, that would otherwise not partition into the  
654 particle phase.

655 Which of the measured compounds contribute significantly to the organic particle mass can be inferred by comparing their  
656 signal from the pure gas phase unseeded cases to their signal with seed in the system. Under the assumptions that, for most  
657 HOM-compounds re-evaporation to the gas phase is negligible and that the precursor chemistry is not substantially disturbed  
658 by seed addition, the fraction of signal remaining with seed in the system reflects to which degree the compound is condensing.  
659 **Figure 13** shows the fraction remaining with seed in the system plotted against the molar mass of each individual compound.  
660 The plot includes all closed shell products that were measured with a relative standard deviation of less than 30% for all  
661 measurement phases and depicts the results for both the high and low HO<sub>2</sub>/RO<sub>2</sub> case.



662

663

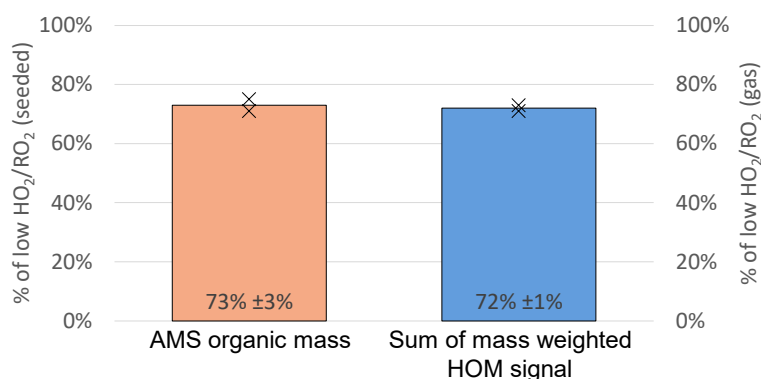
664 **Figure 13: Gas-phase fraction remaining in presence of seed (normalization of all data with  $\alpha$ -pinene OH turnover) for the low (blue)**  
 665 **and high (red)  $\text{HO}_2/\text{RO}_2$  case. Displayed points represent all closed-shell compounds that were detected with relative standard**  
 666 **deviation <30 % in all four experiment phases. Error bars represent result of error propagation (see supplement Sect. [S7S9](#))**

667 Overall, in both cases we observed the same trend. Lighter compounds are not affected by the presence of seed particles, but  
 668 with increasing molar mass the fraction remaining in the gas phase is reduced. A difference between the low and high  $\text{HO}_2/\text{RO}_2$   
 669 case can be observed in the low molar mass range: In the high  $\text{HO}_2/\text{RO}_2$  case many fragmentation products show a higher gas-  
 670 phase fraction remaining up to 1. (In some cases, values larger than 1 were observed, however within the error limits. For the  
 671 error estimation see supplement Sect. [S7S9](#)). Fractions remaining larger than 1 beyond error could be an indication that such  
 672 products have a particle-phase production source. **Figure 13** also shows a critical SVOC/LVOC region for molar masses  
 673 between  $175 \text{ g mol}^{-1}$  and  $250 \text{ g mol}^{-1}$  where neither a fraction remaining of 1 nor complete condensation is observed. The

674 position of this region on the molar mass scale depends on the provided organic mass concentration. The large variation of the  
675 fraction remaining in this small range of molar masses shows that the partitioning coefficients are dependent on the detailed  
676 structure of the compounds and not simply on their molar mass. The semi-volatile and low volatility products represent mainly  
677 higher oxidized fragments and HOM-Mon with less than 8 oxygen.

678 For compounds with a molar mass larger than  $250 \text{ g mol}^{-1}$  a constant fraction remaining is reached in steady state, which is  
679 due to an ongoing production of the compounds. From the condensation behavior shown in **Fig. 13** we conclude that the  
680 compounds heavier than  $230 \text{ g mol}^{-1}$  are expected to be of sufficiently low volatility to be mainly found in the particle phase  
681 for the organic mass present in the system and therefore contribute significantly to the SOA mass formation. Our finding agrees  
682 with the threshold used for low volatility HOM products in Pullinen et al. (2020).

683 Therefore, the signal of all compounds with a molar mass heavier than  $230 \text{ g mol}^{-1}$  was weighted with their molar mass and  
684 summed (see **Eq. (2)**). The ratio of this weighted signal sum at low and high  $\text{HO}_2/\text{RO}_2$  is then a measure of expected SOA  
685 mass loss. The calculation leads to an expected reduction to 72 % (blue bar, **Fig. 14**). This simplified approach leads to a good  
686 agreement with the AMS measurements and can thus explain the reduced particulate organic mass within the errors.



687

688 **Figure 14: Overview of the average, relative change in organic mass observed in the AMS (left y-axis, seeded experiments) and the**  
689 **mass weighted HOM signal observed in the  $\text{NO}_3$ -CIMS (right y-axis, pure gas phase unseeded experiments) between the low and**  
690 **high  $\text{HO}_2/\text{RO}_2$  case (both normalized to  $\alpha$ -pinene OH turnover).**

691 To test for closure between HOM lost and particulate organic mass measured we approximated the upper limit of HOM  
692 concentration in the condensed phase. For this calculation we used the calibration factor determined for sulfuric acid for our  
693  $\text{NO}_3$ -MION-CIMS ( $7.0 \cdot 10^9 \text{ molecules} \cdot \text{cm}^{-3} \cdot \text{ncps}^{-1}$ ) and the relationship between gas and particulate concentration of a  
694 compound in the SAPHIR STAR chamber described in **Eq. (3)**. Again, we considered all compounds with  $M > 230 \text{ g mol}^{-1}$  in  
695 our calculation. The summed mass concentration lost from the gas phase was then compared to the SOA mass measured in the  
696 AMS. This comparison yields a good agreement within the uncertainties. The detailed calculation results can be found in the  
697 supplement (**Fig. S3**). Overall, an agreement within 40 % is achieved for all measurement stages.

698 The comparisons presented above show that we understand the processes governing the SOA formation in our chamber and  
699 that the NO<sub>3</sub>-CIMS measurements are well suited to observe the critical changes to understand the reduction in condensable  
700 organic material when shifting from low to high HO<sub>2</sub>/RO<sub>2</sub>.

## 701 **45 Conclusion**

702 In the presented series of experiments, we achieved a shift from a RO<sub>2</sub>+RO<sub>2</sub> dominated chemistry to a more atmospherically  
703 relevant HO<sub>2</sub>/RO<sub>2</sub> ratio under constant  $\alpha$ -pinene OH turnover. It was shown that moving towards atmospheric HO<sub>2</sub>/RO<sub>2</sub> ratio  
704 affected the SOA formation potential, with the observed organic mass being reduced at high HO<sub>2</sub>/RO<sub>2</sub>. This is in support of  
705 the potential bias towards high SOA yields in chamber studies at low HO<sub>2</sub>/RO<sub>2</sub> as discussed by Schervish and Donahue (2021).

706 Our results confirm that too low HO<sub>2</sub>/RO<sub>2</sub> is one important parameter that can lead to an overestimated SOA yield in laboratory  
707 studies. In a broader picture the results show how important it is to consider the different contributions to the HOM-RO<sub>2</sub> sink  
708 (e.g. HO<sub>2</sub>, RO<sub>2</sub>, NO) when designing experiments and transferring laboratory results to the real atmosphere.

709 The gas-phase observations showed that the SOA reduction at high HO<sub>2</sub>/RO<sub>2</sub> was mainly due to a reduced HOM-Acc formation  
710 which were formed by RO<sub>2</sub>+RO<sub>2</sub> cross reactions in the low HO<sub>2</sub>/RO<sub>2</sub> cases. This prevented contribution to SOA by less  
711 oxidized RO<sub>2</sub> which were scavenged in the HOM-Acc at low HO<sub>2</sub>/RO<sub>2</sub>. Under atmospheric condition such cross reactions are  
712 less important, and such (mixed) accretion products would contribute less to SOA.

713 The overall observed HOM-products were reduced slightly, showing that under certain circumstances RO<sub>2</sub>+HO<sub>2</sub> termination  
714 can impede the HOM formation, mainly by reducing the precursor RO<sub>2</sub> levels and less by impeding the autoxidation itself.  
715 The autoxidation chain (once initiated) runs to a similar oxidation level at both high and low HO<sub>2</sub>/RO<sub>2</sub>. The observed  
716 HOM-Mon products shift significantly between monomer families due to the different termination reaction. A decrease in  
717 carbonyl and alcohol formation from RO<sub>2</sub>+RO<sub>2</sub> and an increase in hydroperoxide formation from RO<sub>2</sub>+HO<sub>2</sub> was observed at  
718 high HO<sub>2</sub>/RO<sub>2</sub>.

719 Furthermore, a reduction in HOM-Frag products, especially with lower carbon numbers, as well as the parity of the C<sub>10</sub>H<sub>15</sub>O<sub>x</sub>  
720 HOM-RO<sub>2</sub> show a reduction in alkoxy radical formation at high HO<sub>2</sub>/RO<sub>2</sub>. The moderate reduction in larger HOM-Frag  
721 products and pinonaldehyde, however, suggest that some alkoxy radical steps are still important. This raises the question of  
722 whether alkoxy radical formation can be facilitated by HO<sub>2</sub>. In the atmosphere such effects are most often overcome whenever  
723 RO<sub>2</sub>+NO is the major alkoxy radical source.

724 Overall, the observed changes in the gas phase could be well explained with the presented generic mechanistic understanding  
725 of HOM formation in the  $\alpha$ -pinene system. The addition of seed demonstrated that the shift towards high HO<sub>2</sub>/RO<sub>2</sub> reduced  
726 the condensable organic mass, stressing the importance of controlling higher order reactions of peroxy radicals which lead to  
727 overemphasis of HOM-Acc product formation at low HO<sub>2</sub>/RO<sub>2</sub> ratios.

728 Furthermore, the seed addition allowed us to determine which products were contributing to the SOA formation and show that  
729 their volatility is a function of molar mass and detailed molecular structure. This revealed a critical mass region in which  
730 compounds have significant fractions in gas and particulate phase. Based on absorptive partitioning theory the volatilities at  
731 which this critical region is found should depend on the organic mass present in the system.

732 Valuable insight about the condensed phase can be gained from HOM gas phase measurements. We inferred conclusions about  
733 the particulate phase from the gas phase measurements and compared them to the direct particle phase observations, finding  
734 good agreements between our expectations and the measurements.

#### 735 **Data availability**

736 All presented data will be available in a repository before the submission of the final manuscript.

#### 737 **Author contribution**

738 TFM, MH and GM conceptualized the study and TFM, YB, SK and SRZ designed the experiments and developed the analysis  
739 methodology. The experiments were performed by YB, SK, VG and SRZ. Instrument deployment and/or data analysis were  
740 performed by YB, SK, HW, RW, JX, AZ, QH, TZ and VG. YB did model calculations of the experiments. AV, SPO, TJB,  
741 MG and MH provided counsel on experiment design and data interpretation. The compiled data set was interpreted by YB and  
742 TFM, and the results were discussed by all co-authors. YB visualized the data and YB and TFM prepared the manuscript. All  
743 co-authors reviewed the manuscript.

#### 744 **Competing interests**

745 The authors declare that they have no conflict of interest.

#### 746 **Financial support**

747 This research has received funding from the European Union's Horizon 2020 research and innovation programme under the  
748 FORCeS grant agreement No 821205, the Federal Ministry of Education and Research (BMBF) Germany under the FONA  
749 Strategy "Research for Sustainability" as part of the implementation of ACTRIS-D under the funding code 01LK200010,  
750 Vetenskapsrådet (VR, grant agreement No. 2018-04430), Svenska Forskningsrådet Formas (grant agreement No. 2019-586)  
751 and the Natural Environment Research Council (NERC) UK under the grant agreement No. NE/V012665/1.

752 **References**

- 753 Albrecht, S. R., Novelli, A., Hofzumahaus, A., Kang, S., Baker, Y., Mentel, T., Wahner, A., and Fuchs, H.: Measurements of  
754 hydroperoxy radicals (HO<sub>2</sub>) at atmospheric concentrations using bromide chemical ionisation mass spectrometry, *Atmos.*  
755 *Meas. Tech.*, 12, 891-902, <https://doi.org/10.5194/amt-12-891-2019>, 2019.
- 756 Atkinson, R. and Arey, J.: Atmospheric degradation of volatile organic compounds, *Chem. Rev.*, 103, 4605-4638,  
757 <https://doi.org/10.1021/cr0206420>, 2003.
- 758 Berndt, T.: Peroxy Radical Processes and Product Formation in the OH Radical-Initiated Oxidation of  $\alpha$ -Pinene for Near-  
759 Atmospheric Conditions, *J. Phys. Chem. A*, 125, 9151-9160, <https://doi.org/10.1021/acs.jpca.1c05576>, 2021.
- 760 Berndt, T., Mentler, B., Scholz, W., Fischer, L., Herrmann, H., Kulmala, M., and Hansel, A.: Accretion product formation  
761 from ozonolysis and OH radical reaction of  $\alpha$ -pinene: mechanistic insight and the influence of isoprene and ethylene, *Environ.*  
762 *Sci. Technol.*, 52, 11069-11077, <https://doi.org/10.1021/acs.est.8b02210>, 2018.
- 763 Berndt, T., Richters, S., Jokinen, T., Hyttinen, N., Kurtén, T., Otkjaer, R. V., Kjaergaard, H. G., Stratmann, F., Herrmann, H.,  
764 Sipila, M., Kulmala, M., and Ehn, M.: Hydroxyl radical-induced formation of highly oxidized organic compounds, *Nat.*  
765 *Commun.*, 7, 13677, <https://doi.org/10.1038/ncomms13677>, 2016.
- 766 Bianchi, F., Garmash, O., He, X. C., Yan, C., Iyer, S., Rosendahl, I., Xu, Z. N., Rissanen, M. P., Riva, M., Taipale, R., Sarnela,  
767 N., Petäjä, T., Worsnop, D. R., Kulmala, M., Ehn, M., and Junninen, H.: The role of highly oxygenated molecules (HOMs) in  
768 determining the composition of ambient ions in the boreal forest, *Atmos. Chem. Phys.*, 17, 13819-13831,  
769 <https://doi.org/10.5194/acp-17-13819-2017>, 2017.
- 770 Bianchi, F., Kurtén, T., Riva, M., Mohr, C., Rissanen, M. P., Roldin, P., Berndt, T., Crouse, J. D., Wennberg, P. O., Mentel,  
771 T. F., Wildt, J., Junninen, H., Jokinen, T., Kulmala, M., Worsnop, D. R., Thornton, J. A., Donahue, N., Kjaergaard, H. G., and  
772 Ehn, M.: Highly Oxygenated Organic Molecules (HOM) from Gas-Phase Autoxidation Involving Peroxy Radicals: A Key  
773 Contributor to Atmospheric Aerosol, *Chem. Rev.*, 119, 3472-3509, <https://doi.org/10.1021/acs.chemrev.8b00395>, 2019.
- 774 Cox, R. A., Ammann, M., Crowley, J. N., Herrmann, H., Jenkin, M. E., McNeill, V. F., Mellouki, A., Troe, J., and Wallington,  
775 T. J.: Evaluated kinetic and photochemical data for atmospheric chemistry: Volume VII – Criegee intermediates, *Atmos.*  
776 *Chem. Phys.*, 20, 13497-13519, <https://doi.org/10.5194/acp-20-13497-2020>, 2020.
- 777 Crouse, J. D., Nielsen, L. B., Jørgensen, S., Kjaergaard, H. G., and Wennberg, P. O.: Autoxidation of organic compounds in  
778 the atmosphere, *J. Phys. Chem. Lett.*, 4, 3513-3520, <https://doi.org/10.1021/jz4019207>, 2013.
- 779 [Docherty, K. S. and Ziemann, P. J.: Effects of stabilized criegee intermediate and OH radical scavengers on aerosol formation](https://doi.org/10.1080/02786820300930)  
780 [from reactions of  \$\beta\$ -pinene with O<sub>3</sub>, \*Aerosol Sci. Tech.\*, 37, 877-891, <https://doi.org/10.1080/02786820300930>, 2003.](https://doi.org/10.1080/02786820300930)
- 781 Eddingsaas, N., Loza, C., Yee, L., Seinfeld, J., and Wennberg, P.:  $\alpha$ -Pinene photooxidation under controlled chemical  
782 conditions – Part 1: Gas-phase composition in low- and high-NO<sub>x</sub> environments, *Atmos. Chem. Phys.*, 12, 6489-6504,  
783 <https://doi.org/10.5194/acp-12-6489-2012>, 2012.
- 784 Ehn, M., Thornton, J. A., Kleist, E., Sipila, M., Junninen, H., Pullinen, I., Springer, M., Rubach, F., Tillmann, R., Lee, B.,  
785 Lopez-Hilfiker, F., Andres, S., Acir, I. H., Rissanen, M., Jokinen, T., Schobesberger, S., Kangasluoma, J., Kontkanen, J.,  
786 Nieminen, T., Kurtén, T., Nielsen, L. B., Jørgensen, S., Kjaergaard, H. G., Canagaratna, M., Maso, M. D., Berndt, T., Petaja,  
787 T., Wahner, A., Kerminen, V. M., Kulmala, M., Worsnop, D. R., Wildt, J., and Mentel, T. F.: A large source of low-volatility  
788 secondary organic aerosol, *Nature*, 506, 476-479, <https://doi.org/10.1038/nature13032>, 2014.



- 789 Eisele, F. and Tanner, D.: Measurement of the gas phase concentration of H<sub>2</sub>SO<sub>4</sub> and methane sulfonic acid and estimates of  
790 H<sub>2</sub>SO<sub>4</sub> production and loss in the atmosphere, *J. Geophys. Res. Atmos.*, 98, 9001-9010, <https://doi.org/10.1029/93JD00031>,  
791 1993.
- 792 Fantechi, G., Vereecken, L., and Peeters, J.: The OH-initiated atmospheric oxidation of pinonaldehyde: Detailed theoretical  
793 study and mechanism construction, *Phys. Chem. Chem. Phys.*, 4, 5795-5805, <https://doi.org/10.1039/B205901K> 2002.
- 794 Guo, Y., Shen, H., Pullinen, I., Luo, H., Kang, S., Vereecken, L., Fuchs, H., Hallquist, M., Acir, I. H., Tillmann, R., Rohrer,  
795 F., Wildt, J., Kiendler-Scharr, A., Wahner, A., Zhao, D. F., and Mentel, T. F.: Identification of highly oxygenated organic  
796 molecules and their role in aerosol formation in the reaction of limonene with nitrate radical, *Atmos. Chem. Phys.*, 22, 11323-  
797 11346, <https://doi.org/10.5194/acp-22-11323-2022>, 2022.
- 798 Hallquist, M., Wenger, J. C., Baltensperger, U., Rudich, Y., Simpson, D., Claeys, M., Dommen, J., Donahue, N. M., George,  
799 C., Goldstein, A. H., Hamilton, J. F., Herrmann, H., Hoffmann, T., Iinuma, Y., Jang, M., Jenkin, M. E., Jimenez, J. L., Kiendler-  
800 Scharr, A., Maenhaut, W., McFiggans, G., Mentel, T. F., Monod, A., Prévôt, A. S. H., Seinfeld, J. H., Surratt, J. D., Szmigielski,  
801 R., and Wildt, J.: The formation, properties and impact of secondary organic aerosol: current and emerging issues, *Atmos.*  
802 *Chem. Phys.*, 9, 5155-5236, <https://doi.org/10.5194/acp-9-5155-2009>, 2009.
- 803 Hantschke, L. L.: Oxidation of monoterpenes studied in atmospheric simulation chambers, Forschungszentrum Jülich GmbH,  
804 Zentralbibliothek, Verlag, 2022.
- 805 Hasson, A. S., Kuwata, K. T., Arroyo, M. C., and Petersen, E. B.: Theoretical studies of the reaction of hydroperoxy radicals  
806 (HO<sub>2</sub>) with ethyl peroxy (CH<sub>3</sub>CH<sub>2</sub>O<sub>2</sub>), acetyl peroxy (CH<sub>3</sub>C(O)O<sub>2</sub>), and acetonyl peroxy (CH<sub>3</sub>C(O)CH<sub>2</sub>O<sub>2</sub>) radicals, *J.*  
807 *Photochem. Photobiol. A*, 176, 218-230, <https://doi.org/10.1016/j.jphotochem.2005.08.012>, 2005.
- 808 Henry, K. M., Lohaus, T., and Donahue, N. M.: Organic aerosol yields from  $\alpha$ -pinene oxidation: bridging the gap between  
809 first-generation yields and aging chemistry, *Environ. Sci. Technol.*, 46, 12347-12354, <https://doi.org/10.1021/es302060y>,  
810 2012.
- 811 Hidy, G.: Atmospheric chemistry in a box or a bag, *Atmos.*, 10, 401, <https://doi.org/10.3390/atmos10070401>, 2019.
- 812 Hyttinen, N., Otkjær, R. V., Iyer, S., Kjaergaard, H. G., Rissanen, M. P., Wennberg, P. O., and Kurtén, T.: Computational  
813 comparison of different reagent ions in the chemical ionization of oxidized multifunctional compounds, *J. Phys. Chem. A*,  
814 122, 269-279, <https://doi.org/10.1021/acs.jpca.7b10015>, 2018.
- 815 Iyer, S., Reiman, H., Møller, K. H., Rissanen, M. P., Kjaergaard, H. G., and Kurtén, T.: Computational investigation of RO<sub>2</sub>+  
816 HO<sub>2</sub> and RO<sub>2</sub>+ RO<sub>2</sub> reactions of monoterpene derived first-generation peroxy radicals leading to radical recycling, *J. Phys.*  
817 *Chem. A*, 122, 9542-9552, <https://doi.org/10.1021/acs.jpca.8b09241>, 2018.
- 818 Iyer, S., Rissanen, M. P., Valiev, R., Barua, S., Krechmer, J. E., Thornton, J., Ehn, M., and Kurtén, T.: Molecular mechanism  
819 for rapid autoxidation in  $\alpha$ -pinene ozonolysis, *Nat. Commun.*, 12, 878, <https://doi.org/10.1038/s41467-021-21172-w>, 2021.
- 820 Jenkin, M. E., Saunders, S. M., and Pilling, M. J.: The tropospheric degradation of volatile organic compounds: a protocol for  
821 mechanism development, *Atmos. Environ.*, 31, 81-104, [https://doi.org/10.1016/S1352-2310\(96\)00105-7](https://doi.org/10.1016/S1352-2310(96)00105-7), 1997.
- 822 Jenkin, M. E., Valorso, R., Aumont, B., and Rickard, A. R.: Estimation of rate coefficients and branching ratios for reactions  
823 of organic peroxy radicals for use in automated mechanism construction, *Atmos. Chem. Phys.*, 19, 7691-7717,  
824 <https://doi.org/10.5194/acp-19-7691-2019>, 2019.

- 825 Johnson, D. and Marston, G.: The gas-phase ozonolysis of unsaturated volatile organic compounds in the troposphere, Chem.  
826 Soc. Rev., 37, 699-716, <https://doi.org/10.1039/B704260B> 2008.
- 827 Junninen, H., Ehn, M., Petäjä, T., Luosujärvi, L., Kotiaho, T., Kostianinen, R., Rohner, U., Gonin, M., Fuhrer, K., Kulmala, M.,  
828 and Worsnop, D. R.: A high-resolution mass spectrometer to measure atmospheric ion composition, Atmos. Meas. Tech., 3,  
829 1039-1053, <https://doi.org/10.5194/amt-3-1039-2010>, 2010.
- 830 Kang, S.: Formation of highly oxygenated organic molecules from  $\alpha$ -pinene photochemistry, Forschungszentrum Jülich  
831 GmbH, 2021.
- 832 [Keyword, M., Kroll, J., Varutbangkul, V., Bahreini, R., Flagan, R., and Seinfeld, J.: Secondary organic aerosol formation from  
833 cyclohexene ozonolysis: Effect of OH scavenger and the role of radical chemistry, Environ. Sci. Technol., 38, 3343-3350,  
834 https://doi.org/10.1021/es049725j, 2004.](https://doi.org/10.1021/es049725j)
- 835 [Khan, M., Cooke, M., Utembe, S., Archibald, A., Derwent, R., Jenkin, M. E., Morris, W., South, N., Hansen, J., Francisco, J.,  
836 Percival, C. J., and Shallcross, D. E.: Global analysis of peroxy radicals and peroxy radical-water complexation using the  
837 STOCHEM-CRI global chemistry and transport model, Atmospheric Environment, 106, 278-287,  
838 https://doi.org/10.1016/j.atmosenv.2015.02.020, 2015.](https://doi.org/10.1016/j.atmosenv.2015.02.020)
- 839 Kiendler-Scharr, A., Wildt, J., Maso, M. D., Hohaus, T., Kleist, E., Mentel, T. F., Tillmann, R., Uerlings, R., Schurr, U., and  
840 Wahner, A.: New particle formation in forests inhibited by isoprene emissions, Nature, 461, 381-384,  
841 <https://doi.org/10.1038/nature08292>, 2009.
- 842 McFiggans, G., Mentel, T. F., Wildt, J., Pullinen, I., Kang, S., Kleist, E., Schmitt, S., Springer, M., Tillmann, R., Wu, C., Zhao,  
843 D., Hallquist, M., Faxon, C., Le Breton, M., Hallquist, A. M., Simpson, D., Bergstrom, R., Jenkin, M. E., Ehn, M., Thornton,  
844 J. A., Alfarra, M. R., Bannan, T. J., Percival, C. J., Priestley, M., Topping, D., and Kiendler-Scharr, A.: Secondary organic  
845 aerosol reduced by mixture of atmospheric vapours, Nature, 565, 587-593, <https://doi.org/10.1038/s41586-018-0871-y>, 2019.
- 846 Mentel, T., Springer, M., Ehn, M., Kleist, E., Pullinen, I., Kurtén, T., Rissanen, M., Wahner, A., and Wildt, J.: Formation of  
847 highly oxidized multifunctional compounds: autoxidation of peroxy radicals formed in the ozonolysis of alkenes—deduced  
848 from structure–product relationships, Atmos. Chem. Phys., 15, 6745-6765, <https://doi.org/10.5194/acp-15-6745-2015>, 2015.
- 849 Mentel, T. F., Wildt, J., Kiendler-Scharr, A., Kleist, E., Tillmann, R., Dal Maso, M., Fisseha, R., Hohaus, T., Spahn, H.,  
850 Uerlings, R., Wegener, R., Griffiths, P. T., Dinar, E., Rudich, Y., and Wahner, A.: Photochemical production of aerosols from  
851 real plant emissions, Atmos. Chem. Phys., 9, 4387-4406, <https://doi.org/10.5194/acp-9-4387-2009>, 2009.
- 852 Mohr, C., Thornton, J. A., Heitto, A., Lopez-Hilfiker, F. D., Lutz, A., Riipinen, I., Hong, J., Donahue, N. M., Hallquist, M.,  
853 Petaja, T., Kulmala, M., and Yli-Juuti, T.: Molecular identification of organic vapors driving atmospheric nanoparticle growth,  
854 Nat. Commun., 10, 4442, <https://doi.org/10.1038/s41467-019-12473-2>, 2019.
- 855 [Otkjaer, R. V., Jakobsen, H. H., Tram, C. M., and Kjaergaard, H. G.: Calculated Hydrogen Shift Rate Constants in Substituted  
856 Alkyl Peroxy Radicals, J. Phys. Chem. A, 122, 8665-8673, https://doi.org/10.1021/acs.jpca.8b06223, 2018.](https://doi.org/10.1021/acs.jpca.8b06223)
- 857 Piletic, I. R. and Kleindienst, T. E.: Rates and yields of unimolecular reactions producing highly oxidized peroxy radicals in  
858 the OH-induced autoxidation of  $\alpha$ -pinene,  $\beta$ -pinene, and limonene, J. Phys. Chem. A, 126, 88-100,  
859 <https://doi.org/10.1021/acs.jpca.1c07961>, 2022.
- 860 Pullinen, I., Schmitt, S., Kang, S., Sarrafzadeh, M., Schlag, P., Andres, S., Kleist, E., Mentel, T. F., Rohrer, F., Springer, M.,  
861 Tillmann, R., Wildt, J., Wu, C., Zhao, D., Wahner, A., and Kiendler-Scharr, A.: Impact of NO<sub>x</sub> on secondary organic aerosol

- 862 (SOA) formation from  $\alpha$ -pinene and  $\beta$ -pinene photooxidation: the role of highly oxygenated organic nitrates, *Atmos. Chem.*  
863 *Phys.*, 20, 10125-10147, <https://doi.org/10.5194/acp-20-10125-2020>, 2020.
- 864 Richter, F., Ostertag, R., Ammerlahn, G., Behrle, E., Baumann, M., and Kobel, M.: Beilstein's handbook of organic chemistry.  
865 Third supplement, covering the literature from 1930-1949, 1955.
- 866 Rissanen, M. P., Mikkilä, J., Iyer, S., and Hakala, J.: Multi-scheme chemical ionization inlet (MION) for fast switching of  
867 reagent ion chemistry in atmospheric pressure chemical ionization mass spectrometry (CIMS) applications, *Atmos. Meas.*  
868 *Tech.*, 12, 6635-6646, <https://doi.org/10.5194/amt-12-6635-2019>, 2019.
- 869 Rissanen, M. P., Kurtén, T., Sipila, M., Thornton, J. A., Kangasluoma, J., Sarnela, N., Junninen, H., Jorgensen, S., Schallhart,  
870 S., Kajos, M. K., Taipale, R., Springer, M., Mentel, T. F., Ruuskanen, T., Petaja, T., Worsnop, D. R., Kjaergaard, H. G., and  
871 Ehn, M.: The formation of highly oxidized multifunctional products in the ozonolysis of cyclohexene, *J. Am. Chem. Soc.*, 136,  
872 15596-15606, <https://doi.org/10.1021/ja507146s>, 2014.
- 873 Roldin, P., Ehn, M., Kurtén, T., Olenius, T., Rissanen, M. P., Sarnela, N., Elm, J., Rantala, P., Hao, L., Hyttinen, N., Heikkinen,  
874 L., Worsnop, D. R., Pichelstorfer, L., Xavier, C., Clusius, P., Öström, E., Petäjä, T., Kulmala, M., Vehkamäki, H., Virtanen,  
875 A., Riipinen, I., and Boy, M.: The role of highly oxygenated organic molecules in the Boreal aerosol-cloud-climate system,  
876 *Nat. Commun.*, 10, 4370, <https://doi.org/10.1038/s41467-019-12338-8>, 2019.
- 877 Sanchez, J., Tanner, D. J., Chen, D., Huey, L. G., and Ng, N. L.: A new technique for the direct detection of HO<sub>2</sub> radicals  
878 using bromide chemical ionization mass spectrometry (Br-CIMS): initial characterization, *Atmos. Meas. Tech.*, 9, 3851-3861,  
879 <https://doi.org/10.5194/amt-9-3851-2016>, 2016.
- 880 Sarrafzadeh, M., Wildt, J., Pullinen, I., Springer, M., Kleist, E., Tillmann, R., Schmitt, S. H., Wu, C., Mentel, T. F., Zhao, D.,  
881 Hastie, D. R., and Kiendler-Scharr, A.: Impact of NO<sub>x</sub> and OH on secondary organic aerosol formation from  $\beta$ -pinene  
882 photooxidation, *Atmos. Chem. Phys.*, 16, 11237-11248, <https://doi.org/10.5194/acp-16-11237-2016>, 2016.
- 883 Saunders, S. M., Jenkin, M. E., Derwent, R., and Pilling, M.: Protocol for the development of the Master Chemical Mechanism,  
884 MCM v3 (Part A): tropospheric degradation of non-aromatic volatile organic compounds, *Atmos. Chem. Phys.*, 3, 161-180,  
885 <https://doi.org/10.5194/acp-3-161-2003>, 2003.
- 886 Schervish, M. and Donahue, N. M.: Peroxy radical kinetics and new particle formation, *Environ. Sci. Atmos.*, 1, 79-92,  
887 <https://doi.org/10.1039/d0ea00017e>, 2021.
- 888 Shen, H., Vereecken, L., Kang, S., Pullinen, I., Fuchs, H., Zhao, D., and Mentel, T. F.: Unexpected significance of a minor  
889 reaction pathway in daytime formation of biogenic highly oxygenated organic compounds, *Sci. Adv.*, 8, eabp8702,  
890 <https://doi.org/10.1126/sciadv.abp8702>, 2022.
- 891 Shen, H., Zhao, D., Pullinen, I., Kang, S., Vereecken, L., Fuchs, H., Acir, I. H., Tillmann, R., Rohrer, F., Wildt, J., Kiendler-  
892 Scharr, A., Wahner, A., and Mentel, T. F.: Highly Oxygenated Organic Nitrates Formed from NO(3) Radical-Initiated  
893 Oxidation of  $\beta$ -Pinene, *Environ. Sci. Technol.*, 55, 15658-15671, <https://doi.org/10.1021/acs.est.1c03978>, 2021.
- 894 Shilling, J. E., Chen, Q., King, S. M., Rosenoern, T., Kroll, J. H., Worsnop, D. R., DeCarlo, P. F., Aiken, A. C., Sueper, D.,  
895 Jimenez, J. L., and Martin, S. T.: Loading-dependent elemental composition of  $\alpha$ -pinene SOA particles, *Atmos. Chem. Phys.*,  
896 9, 771-782, <https://doi.org/10.5194/acp-9-771-2009>, 2009.
- 897 Vereecken, L. and Nozière, B.: H migration in peroxy radicals under atmospheric conditions, *Atmos. Chem. Phys.*, 20, 7429-  
898 7458, <https://doi.org/10.5194/acp-20-7429-2020>, 2020.

- 899 [Vereecken, L.](#), Müller, J.-F., and Peeters, J.: Low-volatility poly-oxygenates in the OH-initiated atmospheric oxidation of  $\alpha$ -  
900 pinene: impact of non-traditional peroxy radical chemistry, *Phys. Chem. Chem. Phys.*, 9, 5241-5248,  
901 <https://doi.org/10.1039/b708023a>, 2007.
- 902 Wildt, J., Mentel, T. F., Kiendler-Scharr, A., Hoffmann, T., Andres, S., Ehn, M., Kleist, E., Müsgen, P., Rohrer, F., Rudich,  
903 Y., Springer, M., Tillmann, R., and Wahner, A.: Suppression of new particle formation from monoterpene oxidation by NO<sub>x</sub>,  
904 *Atmos. Chem. Phys.*, 14, 2789-2804, <https://doi.org/10.5194/acp-14-2789-2014>, 2014.
- 905 Xu, L., Møller, K. H., Crouse, J. D., Otkjær, R. V., Kjaergaard, H. G., and Wennberg, P. O.: Unimolecular reactions of peroxy  
906 radicals formed in the oxidation of  $\alpha$ -pinene and  $\beta$ -pinene by hydroxyl radicals, *J. Phys. Chem. A*, 123, 1661-1674,  
907 <https://doi.org/10.1021/acs.jpca.8b11726>, 2019.  
908